UNIVERSITA' DEGLI STUDI DI VERONA

DEPARTMENT OF
Medicine
GRADUATE SCHOOL OF

Clinical and Experimental Biomedical Sciences

DOCTORAL PROGRAM IN

Life and Health Sciences

WITH THE FINANCIAL CONTRIBUTION OF
(NAME IF THE FUNDING INSTITUTION)

Zunyi Medical University

Cycle / year (1° year of attendance) 37°

TITLE OF THE DOCTORAL THESIS

_ **The Calcium Sensing Receptor Role in Cervical Cancer Cells**

S.S.D. __MEDS 46D_____
(Please complete this space with the S.S.D. of your thesis – mandatory information) *

Coordinator: Prof. Davide Gatti

Signature _____

Tutor: Prof.ssa Anna Chiarini

Signature _____

Doctoral Student: Dott. Zhang Tianhua

Signature _____

Table of Contents

List of Abbreviations

CaSR	Calcium-sensing receptor
HPV	Human papillomavirus
HR-HPVs	High-risk human papillomaviruses
p53	Tumor suppressor protein
pRb	Retinoblastoma protein
GPCR	G-protein-coupled receptor
PTH	Parathyroid hormone
ECD	Extracellular N-terminal domain
TM	Transmembrane
ICD	Intracellular C-terminal domain
mGluRs	Metabotropic glutamate receptor
ER	Endoplasmic reticulum
G proteins	Guanine nucleotide-binding proteins
PLC	Phospholipase C
IP3	Inositol trisphosphate
DAG	Diacylglycerol
PKC	Protein kinase C
PKA	Protein kinase A
JNK	C-Jun N-terminal kinase
PI3K	Phosphoinositide 3-kinase
AKT	A protein kinase
mTOR	Mechanistic target of rapamycin
NPS-2143	CaSR antagonist
Calhex 231	CaSR antagonist
Gd^{3+}	Gadolinium ion, a CaSR agonist
Ly294002	A PI3K inhibitor
KN-93	An inhibitor of calmodulin-dependent protein kinase II (CaMKII)
Torin-1	mTOR kinase inhibitor

SiHa	A cervical cancer cell line
C33A	A cervical cancer cell line
HaCaT	Spontaneously transformed keratinocyte cell line derived from adult human skin
FBS	Fetal Bovine Serum
PBS	Phosphate Buffered Saline
TBS	Tris Buffered Saline
SDS-PAGE	Sodium Dodecyl Sulfate-Polyacrylamide Gel Electrophoresis
WB	Western blotting
AO/EB	Acridine orange/Ethidium Bromide
dsDNA	Double-stranded DNA
ATM	Ataxia telangiectasia mutated
ERK1/2	Extracellular signal-regulated kinases 1/2
TAK1	Transforming growth factor-β-activated kinase 1
CaMKII	Calmodulin-dependent protein kinase II

The Calcium Sensing Receptor Role in Cervical Cancer Cells

Abstract

Background: Cervical cancer remains a leading cause of cancer-related mortality among women worldwide. The calcium-sensing receptor (CaSR), a key regulator of cellular calcium homeostasis, is implicated in various physiological processes, including cell proliferation and apoptosis. However, the role of CaSR in cervical cancer and its associated signaling pathways remains insufficiently explored. This study aims to investigate the effects of CaSR and its antagonists on the proliferation and apoptosis of cervical cancer cell lines and to elucidate the underlying molecular mechanisms.

Method: This study investigated the effects of NPS-2143 on cellular activity, protein expression, and apoptosis signaling pathways in C4-1 cervical cancer cells. C-4 1, SiHa, C-33A, and HaCaT cell lines were cultured under standardized conditions to examine cellular responses to varying concentrations of NPS-2143. Cellular viability was assessed using the Celltiter Blue™ Assay, revealing dose-dependent metabolic activity alterations. Protein extraction and quantification were performed, followed by SDS-PAGE and Western blotting to analyze specific protein expression levels. The RayBio™ Human Apoptosis Signaling Pathway Array identified phosphorylated and cleaved proteins associated with apoptosis. Additionally, dsDNA content was measured using Quant-iT™ PicoGreen™ assay, and AO/EB staining distinguished live and apoptotic cells under fluorescence microscopy. Caspase-3 activity was quantified via fluorometric analysis to evaluate enzymatic activation.

Results: We demonstrated that CaSR is highly expressed in cervical cancer cell lines, including C4-1, Siha, C33A, and HaCaT cells. Using CaSR antagonists, NPS-2143 and Calhex 231, significantly inhibited C4-1 cell proliferation and induced apoptosis. This was evidenced by reduced cell viability, morphological changes, and increased executioner caspase-3 activity. The apoptotic effect of NPS-2143 was further confirmed by a protein array analysis of the human apoptosis signaling pathway, revealing significant alterations in key apoptosis-related proteins. Additionally, NPS-2143

downregulated the expression of HPV-related proteins E6 and E7 and inhibited the PI3K/AKT/mTOR signaling pathway. In contrast, the CaSR agonist Gd3+ promoted C4-1 cell proliferation, reinforcing the specificity of the antagonistic effects of NPS-2143 and Calhex 231. Moreover, treatment with Ly294002, a PI3K inhibitor, and Torin-1, an mTOR inhibitor, induced apoptosis, highlighting the crucial role of the PI3K/AKT/mTOR pathway in mediating the pro-apoptotic effects of CaSR antagonism.

Conclusion: This study explores the role of the calcium-sensing receptor (CaSR) in cervical cancer, highlighting its impact on cell proliferation and apoptosis. CaSR antagonists, NPS-2143 and Calhex 231, demonstrated anti-proliferative and pro-apoptotic effects, with NPS-2143 inducing dose-dependent apoptosis and affecting key cell cycle regulators. The study also reveals that NPS-2143 reduces HPV-associated oncogenes E6 and E7 expression, offering a dual therapeutic approach. Additionally, the PI3K/AKT/mTOR pathway was implicated in the pro-apoptotic effects of CaSR antagonism. These findings suggest CaSR antagonists as promising candidates for treating HPV-positive cervical cancers, warranting further investigation to confirm their clinical efficacy.

Key words: cervical cancer, calcium-sensing receptor, apoptosis, NPS-2143, Calhex 231, HPV, C4-1 cell PI3K/AKT/mTOR signaling

Introduction

1. Background of cervical cancer

Cervical cancer remains a critical global health issue, disproportionately impacting women in low- and middle-income countries[1]. Despite advancements in preventive and therapeutic strategies, it is the fourth most prevalent cancer among women globally. In 2020 alone, cervical cancer accounted for approximately 604,000 new diagnoses and 342,000 fatalities, highlighting its enduring burden on public health systems[2,3].

The pathogenesis of cervical cancer is strongly associated with persistent infection by high-risk human papillomaviruses (HR-HPVs), particularly HPV16 and HPV18, which are implicated in nearly 70% of cases[4,5]. Cervical carcinogenesis involves a multistep progression initiated by HPV infection, culminating in the integration of viral DNA into the host genome[6]. This integration promotes the overexpression of viral oncoproteins E6 and E7, which subvert the tumor-suppressive functions of p53 and retinoblastoma protein (pRb), respectively[7,8]. These molecular alterations induce genomic instability, uncontrolled cellular proliferation, and resistance to apoptosis, hallmarks of malignant transformation. Additional cofactors, including tobacco use, prolonged oral contraceptive exposure, immunosuppression, and co-infections with other sexually transmitted pathogens, further exacerbate the risk and progression of cervical cancer[9].

Cervical cancer is a predominant malignancy among women, with its etiology firmly linked to infection with human papillomavirus (HPV)[4]. Human papillomaviruses from the family Papillomaviridae belong to a category of small, non-enveloped circular double-stranded DNA viruses measuring 50–55 nm in diameter[10]. Human papillomaviruses have been divided into five genera: alpha (65 types, including HPV16, 18, 31, 33, etc.), beta (53 types, including HPV5, 9, 49, etc.), gamma (98 types, including HPV4, 48, 50, etc.), mu (3 types, including HPV1, HPV63, and HPV 204), and nu[11]. The International Agency for Research on Cancer (IARC) has designated the Human Papillomavirus types 16, 18, 31, 33, 35, 39, 45, 51, 52, 56, 58, 59, and 66 as high-risk Human Papillomaviruses (HR-HPV). The human papillomavirus types 6, 11, 40, 42, 43, 44, -53, 54, 61, 72, and 81 are categorized as low-risk (LR-HPV) HPVs. In 60.5% of cervical cancer cases, HPV 16 is unambiguously the most commonly identified genotype, followed by HPV18[6,12].

The relationship between the E6 and E7 oncoproteins and human papillomavirus (HPV) is pivotal in the development of HPV-associated cancers, particularly cervical cancer[8]. HPV E6 and E7 are viral proteins encoded by the HPV genome and play crucial roles in oncogenesis through their interactions with key cellular proteins. The early coding regions, primarily E6 and E7, are responsible for malignant transformation,

whereas the late coding regions produce structural proteins[13]. However, the E6 and E7 proteins of high-risk HPVs show transforming activity that leads to autonomous or synergistic cell immortalization. Low-risk LR-HPVs have minimal immortalization activity[14]. The best-studied function of HR-HPV E6 is the degradation of the p53 tumor suppressor protein to disrupt pro-apoptotic signaling. Over 50% of all human malignancies have altered or inactivated p53, a sequence-specific DNA binding protein that acts as an effector of DNA damage[15]. In response to a wide range of stressors, it can induce cell-cycle arrest, cellular senescence, and apoptosis through transcriptional control. E6 also targets other apoptosis-related proteins in addition to p53. This includes binding to the host proapoptotic protein Bcl-2 homologous antagonist/killer (BAK) to decrease intrinsic apoptosis signaling. E6 combines with E6-AP to target and degrade BAK, much like p53[16,17]. Similarly, E7-mediated inhibition of retinoblastoma protein (pRb) is a significant step toward achieving unrestrained cell proliferation. pRb–E2F interaction is a mandatory checkpoint for the cells to travel through the G1-S phase transition. The two key oncogenes, E6 and E7, whose constitutive expression promotes carcinogenesis, are necessary for the initial development and subsequent advancement of this kind of cancer[13,18]. Therefore, manipulating these genes is the most effective cervical cancer treatment methodology[19,20].

2. Overview of Calcium-sensing receptor.

Calcium (Ca^{2+}) is one of the most pivotal and versatile intracellular second messengers, orchestrating a myriad of cellular and physiological processes[21]. These include muscle contraction, exocytosis, neurotransmitter release, cell proliferation, and apoptosis, with both short-term signaling and long-term regulatory roles mediated by Ca^{2+} dynamics[22,23]. The extracellular calcium-sensing receptor(CaSR), a class C G-protein-coupled receptor (GPCR), has emerged as a central regulator of calcium homeostasis[24]. Extensive studies employing mRNA probes and antibody-based techniques have demonstrated that CaSR is ubiquitously expressed across various tissues,

extending its functional repertoire beyond regulating systemic calcium balance. Predominantly localized in the parathyroid and thyroid glands and the kidneys, CaSR plays a critical role in maintaining extracellular calcium equilibrium. Beyond these classical sites, its expression in other tissues underscores its involvement in diverse physiological and pathophysiological contexts, broadening its significance as a molecular target for therapeutic exploration[24]. This receptor's ability to sense minute fluctuations in extracellular Ca^{2+} concentration positions it as a key mediator in calcium signaling, linking environmental cues to intracellular responses across multiple biological systems. Its roles in endocrine regulation, cellular signaling, and homeostasis highlight its potential impact on various disease processes[25].

The CaSR plays a pivotal role in maintaining calcium homeostasis by regulating extracellular calcium levels across various tissues[26,27]. The parathyroid glands modulate the secretion of parathyroid hormone (PTH) in response to fluctuations in serum calcium concentrations, thus influencing calcium mobilization from bone, renal calcium reabsorption, and intestinal calcium absorption. The CaSR regulates calcium reabsorption in the kidneys by detecting calcium level changes, ensuring calcium balance is maintained[28,29]. Moreover, the CaSR participates in bone remodeling in bone tissue by modulating osteoclast activity, thus impacting bone density and mineral turnover. This receptor also influences other systems, such as the gastrointestinal tract, where it may contribute to calcium absorption. By integrating signals from extracellular calcium, the CaSR orchestrates a coordinated response to sustain optimal calcium levels, essential for cellular function, neuromuscular activity, and overall metabolic stability[26,30,31].

3. CaSR structure

The CaSR protein, which is 1078 amino acids long, is made up of four primary domains: a large extracellular N terminal domain (ECD), a cysteine-rich domain that connects the ECD to the first transmembrane helix, a seven-transmembrane (TM)

domain, and an intracellular C-terminal domain[32,33]. The vast extracellular domain, seen in many GPCRs, is organized in a Venus-flytrap configuration. The bulk of CaSR ligand binding sites are found in this motif; some are found in the transmembrane domain. Most predictions on the areas involved in ligand binding are made using the X-ray structure of the metabotropic glutamate receptors (mGluRs)[21], which are members of the same GPCR family, as the crystal structure of the CaSR is yet unknown. The ECD is the most common location for naturally occurring mutations[34]. This domain has a signal peptide cleavage site at its N-terminus. Cell surface expression, signaling, and receptor dimerization depend on the conserved cysteine-rich domain[35]. CaSR signaling and surface expression depend on the 216 amino acid intracellular tail[36]. Indeed, homology modeling studies using the crystal structure of the related metabotropic glutamate receptor show that it contains a cavity between its midportion and extracellular aspect. This cavity is the site of binding for positive allosteric modulators like phenylethylamine calcimimetic drugs and negative allosteric modulators like amino alcohol calcitic drugs[37].

The signal peptide directs the CaSR to the endoplasmic reticulum (ER) during biosynthesis, where it undergoes dimerization and is subsequently glycosylated in the Golgi before reaching the cell surface[38,39]. While the CaSR is often found at the cell surface as a homodimer, it may also bind to other proteins such as filamins, dorfin, and β arrestins, as well as form heterodimeric complexes with other GPCRs such as the glutamate receptors or the γ-aminobutyric acid-B receptor 1[40,41]. Although crucial, dimer formation cannot remove the CaSR from the ER pool.

The CaSR receptor is a promiscuous receptor that recognizes a wide range of ligands. The CaSR's conformation changes in response to ligand binding, resulting in the binding and activating related guanine nucleotide-binding proteins (G proteins) and initiating a complicated, G protein-mediated downstream signaling cascade. A wide range of ligands activate CaSR. Type-I or orthosteric ligands activate the receptor directly, but type-II ligands are allosteric modulators that make the receptor more sensitive to type-I ligands. Ca^{2+} is the primary orthosteric physiological ligand of the CaSR[42].The calcium-sensing receptor modulates many downstream signaling cascades by binding distinct G protein subunits. Several parameters, including receptor type,

ligands, intracellular protein concentration, G protein expression and binding affinity, and receptor deactivation rate43, influence the kinetics of G protein activation. Four kinds of G subunits have been identified as involved in CaSR-mediated signaling, triggering complicated downstream pathways ($G_{i/o}$, G_s, $G_{\alpha}q/11$, and $G_{12/13}$)[44]（Fig.1）.

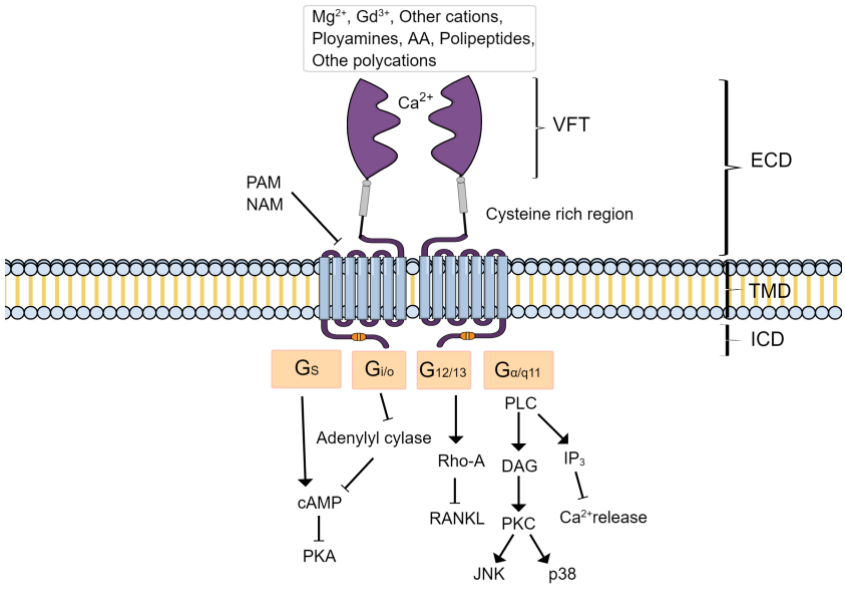

Fig.1. shows G protein activation and downstream signaling of the active CaSR. CaSR ligands include endogenous cations, polyamines, amino acids, pharmaceuticals, and physiological circumstances. The CaSR regulates several critical signaling activities, including intracellular Ca2+ signaling, cAMP production, and protein phosphorylation.

4. The CaSR role in cancer

The potential involvement of CaSR in several cancer types has recently attracted a lot of attention. The calcium-sensing receptor manipulates cell fate by influencing hormone synthesis, proliferation, differentiation, apoptosis, and chemotaxis in addition to its primary function in calcium homeostasis[24]. The ability of CaSR to regulate cell fate suggests that it will significantly impact cancer formation. Surprisingly, the CaSR has consistently attracted interest as an oncogene or tumor suppressor in different cancer[45]. CaSR appears to operate as an oncogene in various malignancies, including prostate, testicular, ovarian, and breast cancer, often by boosting proliferation and

preventing apoptosis[46]. The mechanics, however, are not entirely understood. Conversely, there is some indication that the CaSR is a key mediator of calcium's anti-tumorigenic actions. However, CaSR expression is diminished or wholly deleted in several cancers, including parathyroid carcinoma[47], colorectal cancer[48], and neuroblastomas[49]. Loss of receptor function in these tumors results in a loss of calcium's protective benefits because a drop in CaSR levels alters both critical aspects of the Ca_i^{2+} response at the single-cell level and the fraction of cells reacting to Ca_o^{2+}. The mechanisms that contribute to the decrease of expression differ between tumors. Both genetic and epigenetic pathways contribute to CaSR silencing in neuroblastomas; in colorectal tumors, epigenetic mechanisms are predominantly responsible for CaSR loss[49,50].

However, the role of CaSR in cervical cancer is not clear. In this study, we explored the expression level of CaSR in cervical cancer cell lines and HaCaT cell lines. The present experiments investigate the protein expression level, cell morphology, viability, and cellular morphology of CaSR in C-41 cells after CaSR calcitic (NPS-2143, Calhex231) treatment. In addition, the involvement of the PI3K/Akt signaling pathway in these effects was analyzed by the Human Apoptosis Signaling Pathway Array Kit.

Materials and Methods

1. Material

1.1 Regents

Name	Source
Bio-Rad protein assay reagent	Bio-Rad (USA)
BSA	Gibco (USA)
DMEM	Gibco (USA)

FBS	Gibco (USA)
PBS	Sigma (USA)
TBS	Sigma (USA)
NPS-2143 hydrochloride	MedChemExpress LLC(USA)
AlamarBlue™ Cell Viability Reagent	Thermo(USA)
T-PER™ Tissue Protein Extraction Reagent	Thermo(USA)
Halt™protease&Phosphatase Inhibitor	Thermo(USA)
Phosphatase inhibitor	Thermo(USA)
Odyssey DLx Imager	LI-COR(USA)
Intercept Blocking Buffer	LI-COR(USA)
iBlot™ Transfer Stack, nitrocellulose, mini size	Thermo(USA)
Anti-CASR (Calcium sensing receptor)	Sigma(USA)
Anti-CyclinD1(H-295)	Santa Cruz Biotechnology(USA)
Anti-CyclinB1(H-433)	Santa Cruz Biotechnology(USA)
Anti-CyclinE(M-20)	Santa Cruz Biotechnology(USA)
Chromatin Condensation/Dead Cell Apoptosis Kit	Invitrogen(USA)
Acridine orange	Invitrogen(USA)
RayBio®C-Series Human Apoptosis Signaling Pathway Array C1	RayBiotech(Italy)
caspase-3 substrate(Ac-DEVD-AMC)	Alexis
Calhex 231	Tocris
Gadolinium	Sigma(USA)
Anti-HPV 18-E6 (N-17)	Santa Cruz Biotechnology(USA)
Anti-HPV 18-E7(N-19)	Santa Cruz Biotechnology(USA)
Ly294002	MedChemExpress LLC(USA)
KN-93	MedChemExpress LLC(USA)

Anti-β-actin(C4)	Santa Cruz Biotechnology(USA)
Torin-1	MedChemExpress LLC(USA)
LDS Sample Buffer(4×)	Invitrogen
TWEEN®20	Sigma(USA)
IRDye®800CW Goat anti-Mouse 926-32210	LI-COR(USA)
IRDye®800CW Goat anti-Rabbit 926-32211	LI-COR(USA)
DMSO	Sigma(USA)
DPBS	Gibco(USA)
Dulbecco's Modified Eagle Medium	Gibco(USA)
Penicillin-Streptomycin	BioWhittaker(USA)
Fetal Bovine Serum	EuroClone(Italy)

1.2 Cells

C4-1(ATCC CRL-1595) cells were bought from ACTT(USA). This cell line contains human papillomavirus type 18 (HPV-18) DNA sequences and expresses HPV-18 RNA. ATCC confirmed that this cell line is positive for the presence of HPV viral DNA sequences via PCR. The culture medium for the C-4 1 cells was Dulbecco's minimum essential medium (DMEM) (94% v/v; Gibco, USA) fortified complements heat-inactivated (at 56 °C for 30 minutes) fetal bovine serum (FBS) (5% v/v; Gibico, USA) and penicillin-streptomycin solution (1% v/v; CAMBREX, Belgium).

SiHa (ICLC: HTL98017) cells were bought from Cell Bank Interlab Cell Line Collection (ICLC) Genoa(Italy). This line was established from fragments of a primary tissue sample obtained from a Japanese patient after surgery and is reported to contain an integrated human papillomavirus type 16 genome (HPV-16, 1 to 2 copies per cell). To make the complete growth medium, using Dulbecco's minimum essential medium (DMEM) (89% v/v; Gibco, USA), add fetal bovine serum (FBS) (10% v/v; Gibico, USA)

and penicillin-streptomycin solution (1% v/v; CAMBREX, Belgium).

C-33A (ICLC HTL02004) was an epithelial cell isolated from the cervix of a 66-year-old white patient with uterine cancer, purchased from Cell Bank Interlab Cell Line Collection (ICLC), Genoa(Italy). The C-33 A cell line is one of a series of lines (see also ATCC CRL-1594 and ATCC CRL-1595) derived by N. Auersperg from cervical cancer biopsies, which are harmful to human papillomavirus DNA and RNA. The C-33A cells were cultured in DMEM (89% v/v; Gibco, USA) supplemented with heat-inactivated FBS (10% v/v; Gibico, USA) and 1% v/v penicillin-streptomycin solution (CAMBREX, Belgium).

HaCaT cells (NO. 300493) were purchased from CLS Cell Lines Service GmbH (Germany). The findings of virus tests using Real-Time PCR were negative. HaCaT cells from adult human skin are spontaneously transformed keratinocytes isolated from histologically normal skin samples and cultivated in vitro. The HaCaT cells were cultured in DMEM (94% v/v; Gibco, USA) supplemented with heat-inactivated FBS (5% v/v; Gibico, USA) and 1% v/v penicillin-streptomycin solution (CAMBREX, Belgium).

2. Methods

2.1 Cell titer Blue Assay

C4-1 cells were seeded into lumox® multiwell, Cell culture plate, 12 well(Sarstedt, Italy) at a density of 30,000 cells per well following enumeration by Scepter™ Handheld Automated Cell Counter(Merck, Italy). The seeding density per well was standardized across all conditions. The cells were kept in 1 ml of DMEM supplemented with 5% FBS. After a 24-hour incubation period, cellular adhesion was completed. The experimental setup encompassed both a control group and several experimental groups. The control group was kept in DMEM, while the experimental groups were treated with different

concentrations (5, 10, 25, 50, and 100 μM) of NPS-2143 added to DMEM supplemented with 5% FBS. The volume of each well was 1 ml. Subsequently, the cells were subjected to an additional 24 hours of incubation. Each experimental condition was replicated in triplicate wells.

Thaw the frozen Celltiter Blue™ Assay Reagent(Promega, Italy) and allow it to equilibrate to room temperature. The Celltiter Blue™ Assay reagent is supplied as a premixed solution and can be directly added to individual wells of a 12-well plate. Subsequently, cells were incubated with the Celltiter Blue™ Assay Reagent(10% of the volume of medium) for a predetermined duration of 2 hours at 37°C in a humidified atmosphere enriched with 5% CO_2. During this incubation period, metabolically active cells undergo an enzymatic reduction of the Celltiter Blue™ Assay Reagent, leading to the conversion of the non-fluorescent resazurin dye into its red fluorescent counterpart, resorufin(Fig.2).

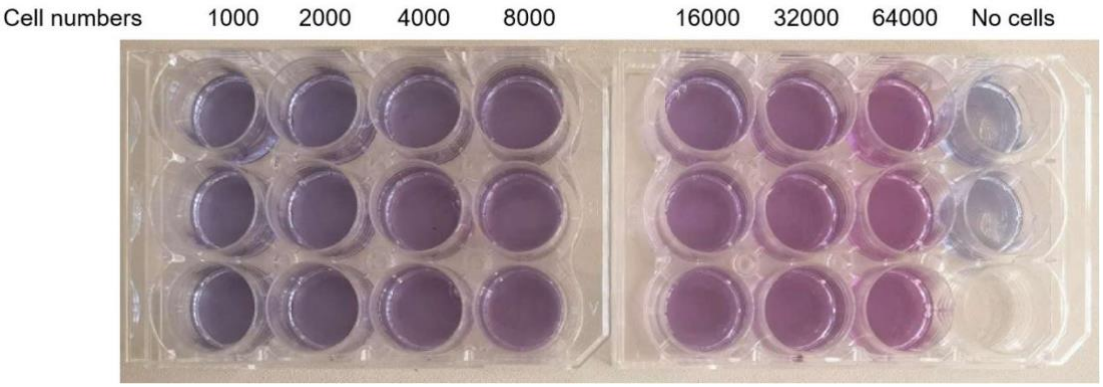

Fig.2. Changes in different amounts of C4-1 after 2 hours of incubation with Celltiter Blue™ Assay.

After the incubation period, the fluorescence of the Celltiter Blue™ was reduced by the cells Celltiter blue. Excitation and emission wavelengths typically used for 560nm and 590nm, respectively, was recorded by means of the Model FP-6200 Spectrofluorometer (JASCO, Japan). The experimental procedure can be seen in Fig.3.

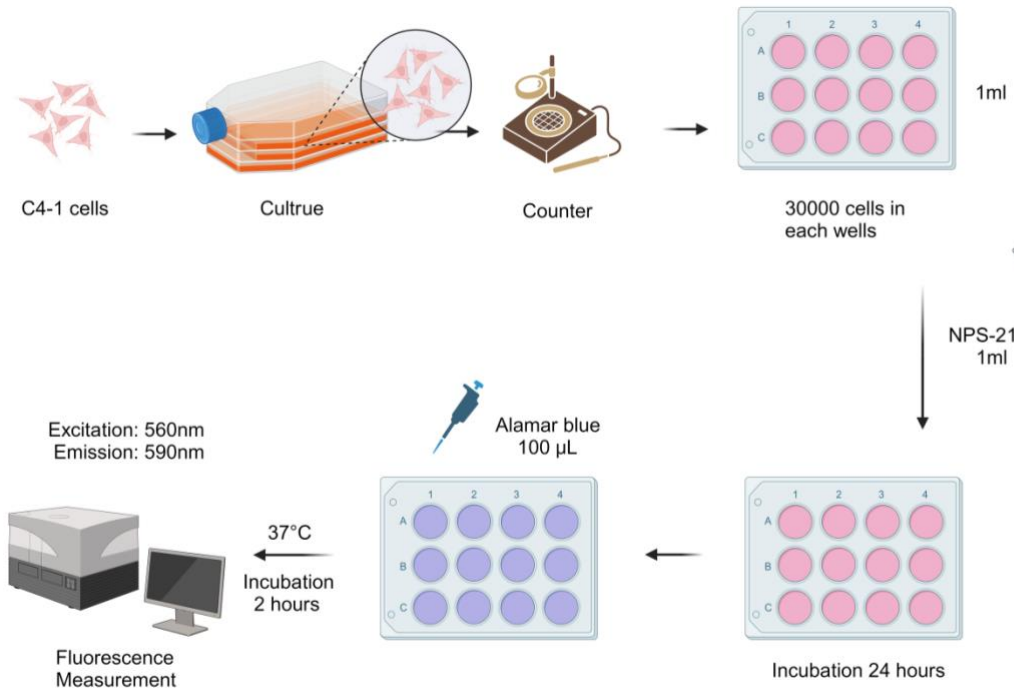

Fig.3. Celltiter Blue™ Assay experimental procedure.

2.2 Protein extraction

400,000 C4-1 cells were seeded in flasks(75cm^2, Sauteed) and maintained in 5% FBS/DMEM. After 24 hours, one flask served as CTR, and the three others, NPS-2143, were added at a concentration of 35 µM from 30min to 24 hours. The cells were then scraped and harvested by centrifugation at 1600 r for 6 minutes, resulting in a cell pellet. The supernatant was then decanted, and PBS was added, followed by thorough mixing. The cells were transferred to a 2ml tube and subjected to further centrifugation to eliminate any remaining medium or impurities. The cellular pellet was then treated with a suitable volume of T-PER buffer (Thermo, USA) plus phosphatase protease and inhibitors(100:1) to lyse the cells. Subsequently, the cells were incubated on ice for 5-30 minutes, allowing the lysis buffer to permeate cell membranes and lysis proteins. Centrifugation at 10,000×g was employed to precipitate insoluble cellular debris and other particulate matter. The resulting supernatant, housing soluble proteins, was cautiously transferred to a tube, avoiding disturbance to the precipitate. The protein content of each sample was determined by means of a Bio-Rad Protein Assay. The

protein standards are mixed with an appropriate volume of the Coomassie dye reagent. The protein concentration of the sample is determined by measuring its absorbance spectrophotometrically at a specific wavelength (595 nm) using a spectrophotometer and comparing it to a standard curve generated from the absorbance values of protein standards(Bovine serum albumin) with known concentrations.

2.3 Western blotting

Sample preparation started with quantification of the protein content using the Bio-Rad protein assay. Subsequently, the sample was denatured and reduced in the SDS Loading Buffer and subjected to a 10-minute incubation in a preheated metal bath set to 85℃. Polyacrylamide gels were then prepared for 10% or 4%-12% SDS-PAGE, with equal amounts of protein samples(10μg-30μg) loaded alongside molecular weight markers to serve as size references.

Electrophoresis was conducted at 80 V, ceasing upon depletion of bromophenol blue from the gel. The separated proteins were then transferred from the gel to an iBlot™ Transfer Stack, nitrocellulose membrane (Thermo, USA) using the iBlot™ Gel Transfer Device, where an electric current facilitated protein migration from the gel to the membrane.

The membrane was wetted in 1 × TBS for 5 minutes; then, the membrane was blocked in an incubation box with Intercept Blocking™ Buffer (LI-COR, USA) for 1 hour at room temperature with gentle shaking.

The primary antibodies were diluted in Intercept Blocking™ Buffer in a range from 1:100 to 1:500. The membrane was incubated overnight at 4℃ with gentle shaking. Then off, the membrane was rinsed with 1 × TBS-T (0.1% Tween 20) on a platform shaker at room temperature for 5 minutes 4 times. IRDye® 800CW Goat anti-Rabbit or anti-Mouse IgG Secondary Antibodies were diluted to a final concentration (1:3000) with Intercept Blocking Buffer plus 0.2% Tween 20. The blot underwent a 1-hour incubation at room temperature with gentle shaking. Subsequently, the membrane was subjected to

four 5-minute rinses with 1× TBS-T (0.1% Tween 20) on a platform shaker at room temperature. Finally, the membrane was rinsed with 1× TBS to eliminate residual Tween 20. The blot was scanned using the Odyssey Imaging System (LI-COR, USA), and the intensity of each band was quantified using the Image Studio Software.

2.4 Human Apoptosis Signaling Pathway.

I used the RayBio^{Tm} Human Apoptosis signaling Pathway Array to identify and quantify phosphorylated or cleaved proteins involved in the signaling pathways related to apoptosis, according to the manufacturer's protocol. Briefly, equal amounts of proteins (i.e., 100 μg) from each experimental group (CTR or NPS-2143-treated groups) were incubated overnight at 4℃ with the membrane antibody arrays, previously blocked for one hour with Intercept^{TM} TBS-blocking buffer (Ll-COR Biosciences GmbH, Germany). After five washing cycles, the membranes were incubated for two hours at room temperature with a mix of array-specific biotin-conjugated primary antibodies diluted 1:250 in Intercept® TBS-blocking buffer. Finally, after five washing cycles, all the membranes were incubated at room temperature for one hour with Dylight800-conjugated streptavidin (dilution1:7500 in Intercept® PBS-blocking buffer, LGC Clinical Diagnostics' KPL, USA). The signals of the various proteins were acquired by an Odissey® scanner (Ll-COR Biosciences GmbH), and the signal intensity was expressed as the sum of the intensity of the individual pixel intensity values for a spot minus the product of the average intensity values of the pixels in the background and the total number of pixels enclosed by the area of the spot-were quantified using the image Studio^{TM} software package (version 5.2, LI-COR Biosciences GmbH). To compare the results across multiple arrays, the values of the favorable control spots from each array were used to normalize the signal responses. The results from three independent experiments were averaged and expressed as mean values ± SDs.

2.5 dsDNA assay

30,000 C4-1 cells were seeded in 12-well plates using 5% FBS DMEM. Some wells served as control, while others were treated with 35μM NPS-2143 for 8, 24, and 48 hours. The control group received regular changes of culture medium, while the experimental group was treated with NPS-2143 35μM in parallel. At the same time, I seeded (10,000, 20,000, 50,000, 100,000) cells to be tended for the dsDNA content and for the preparation of the standard curve. To assess the dsDNA content, the cells were washed twice with PBS. 250μl of deionized water was added to each well to lyse the cells after washing. The plates were frozen at -20°C, and after three cycles of freezing and thawing, the dsDNA content was tested using Quant-iT™ PicoGreen™ dsDNA Reagent (Thermo) according to the supplied protocol. The sample fluorescence was measured using fluorescence fluorescein wavelengths (excitation 480 nm, emission 520 nm).

2.6 Acridine orange/Ethidium Bromide (AO/EB) Staining.

The C4-1 cells were counted using a cell counter, and 400,000 cells were cultured in 10% FBS DMEM. After incubation for 24 hours, the cells were completely attached. Next, NPS2143 35 μM dissolved in 10% FBS DMEM was added, and the cells were incubated for an additional 24 hours. The basal adherent cells were gently scraped off the culture bottle using a scraper, taking care to avoid injuring any cells. The cells were then mixed into the culture medium and introduced into a tube. After centrifugation at 2000r for 8 minutes, the supernatant was removed, and 0.5ml of the cell mixture was retained. Mix gently again.

Prepare a stock solution of acridine orange (AO) and ethidium bromide (EB) in an appropriate solvent concentration. 1ul of Actiodine orange was mixed with 99 ul of PBS, followed by the addition of 2ul of Propidium iodide and thorough mixing(AO/EB). Acridine orange stains both live and dead cells, while ethidium bromide only stains dead cells. By combining the two dyes, it is possible to differentiate between live cells (green

fluorescence) and dead cells (red fluorescence).

Incubate 50 µl of cell suspension with 2 µl of acridine orange/ethidium bromide (AO/EB) solution. Careful mixing. Place 10 µl of cell suspension on a microscopic slide, cover it with a glass coverslip, and examine at least 300 cells under a fluorescence microscope using a fluorescein filter and a 10/40 x objective.

2.7 Caspase 3 Enzymatic Activity Assay

I determined Caspase 3 enzymatic activity was measured in protein lysates (50 µg) by using the fluorogenic substrate N-Acetyl-Asp-Glu-Val-Asp-7-amino-4-methylcoumarin or Ac-DEVD-AMC. The reaction buffer consisted of 25 mM HEPES, 0.1%v/v CHAPS, and 10 mM DTT, pH 7.5. The substrate had a final concentration of 100 µM. After a 2-hour incubation at 37°C, the enzymatic activities were fluorometrically measured at excitation λl380 nm and emission λ460 nm. The results were expressed in arbitrary units calculated as fluorescence values for 50 μg^{-1} protein.

2.8 Data Analysis and Statistics

I analyze the fluorescence intensity data to calculate the relative metabolic activity or cell viability of each treatment condition compared to control wells. I generated graphs or tables to visualize and interpret the results, highlighting any differences in metabolic activity between experimental conditions. I performed statistical analysis using a T-test or one-way ANOVA to determine the significance of differences in metabolic activity between experimental groups and controls.

Results:

1. CaSR is highly expressed in cervical cancer cell lines and HaCaT cells

The protein expression levels of CaSR were assessed in human cervical cancer and HaCaT via western blotting. As shown in Fig. 4, CaSR was significantly expressed in cervical cancer cell lines and HaCaT. Specifically, SiHa and C33A expression levels demonstrated a substantial increase when compared to the C4-1 cell groups, reaching statistical significance (****$p < 0.0001$). Their expression levels were approximately 4.35 and 2.84 times higher than those of the C4-1 cell groups, respectively. Conversely, no significant disparity was observed between HaCaT cells and C4-1 cells. The results show that CaSR is substantially expressed in cervical cancer cell lines and HaCaT cells.

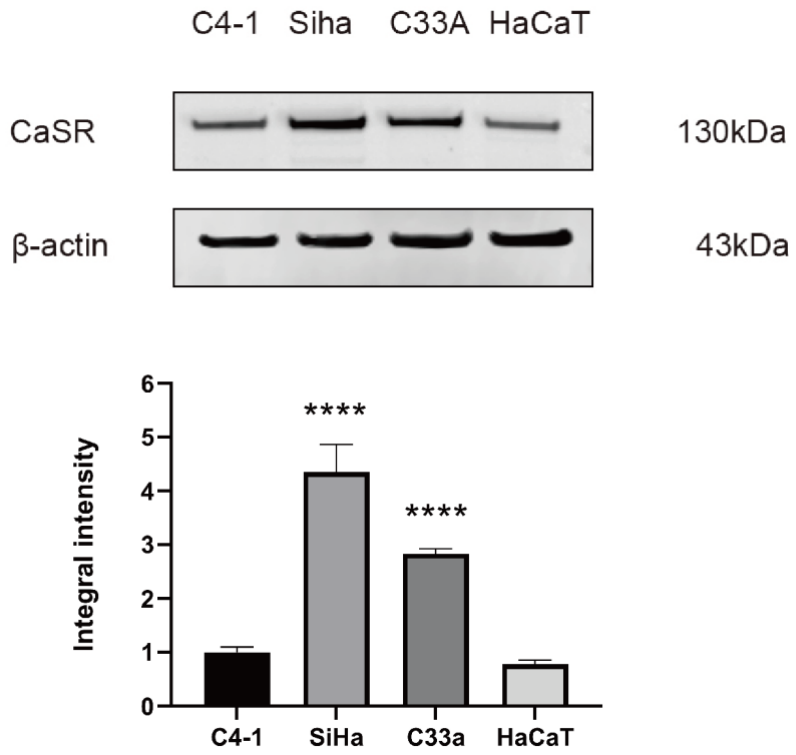

Fig.4. Western blotting and densitometric analysis (arbitrary units normalized of cells to CaSR protein expression) elucidated the expression levels of CaSR protein in cervical cancer cell lines and HaCaT cells. Means ± SD(n=3). Comparison versus C4-1 cells chosen as reference cells. ****$p < 0.0001$ vs. expression of Ca SR in C4-1 cell line.

2. Ca SR antagonist significantly inhibited C4-1 cell proliferation and promoted apoptosis

2.1 NPS-2143 inhibited C4-1 cell proliferation and promoted apoptosis

2.1.1 The viability of C4-1 cells is significantly inhibited by NPS-2143

Under normal conditions, C4-1 proliferated and metabolized Celltiter Blue™ Reagent, giving the results plotted in Fig. 5. A. I found that NPS-2143 inhibited C4-1 cell proliferation in a dose-dependent manner. The IC_{50} value of NPS-2143 for the viability of C4-1 cells was found to be 35.25 μM. All subsequent experiments were performed using 35.25 μM NPS-2143. I defined C4-1 cells growing autonomously for 24 h as the control group (Ctr). No statistically significant difference in cell viability was observed between the Ctr and the 5 and 10 μM NPS-2143 groups. However, a statistically significant difference in cell viability was observed between the 25, 50, and 100 μM NPS-2143 groups compared to the control group (Fig. 5.B).

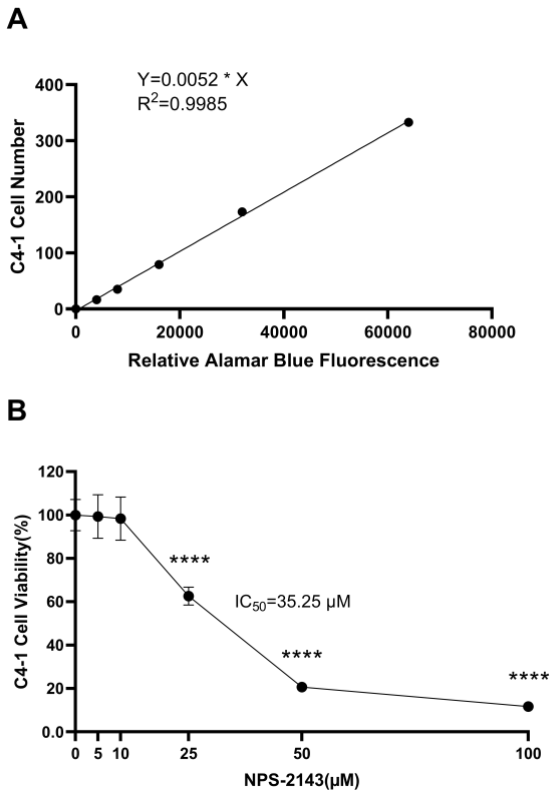

Fig.5. Effect of NPS-2143 on the viability of C4-1 cells after 24h. A) The standard curve for C4-1 cells was measured using Celltiter Blue^{TM} Assay. **B)** Viability of C4-1 cells after treatment with different concentrations of NPS-2143 for 24 hours. The IC_{50} value of NPS-2143 for the viability of C4-1 cells was 35.25 μM.

2.1.2 Cell morphology following 24 hours treatment with NPS-2143

Then, I studied to observe the morphological changes in C4-1 cells during proliferation under the treatment of NPS-2143. When C4-1 cells proliferated, they displayed irregular morphology typified by polygonal shapes and heterogeneous sizes. The nuclei exhibited enlargement and irregular shapes, accompanied by either aggregated or dispersed chromatin and prominent nucleoli. Cellular growth tended towards clustering or aggregation, forming irregularly shaped colonies with isolated cells interspersed in control groups. After a 24-hour treatment period, the morphology of NPS-2143 5 μM and 10 μM groups were very similar to the control group. Whereas the treatment with 25, 50, and 100 μM of NPS-2143 induced observable cell apoptosis.

The emergence of apoptotic bodies, chromatin condensation, cell shrinkage, and bleb formation were evident and shown in Fig.6.

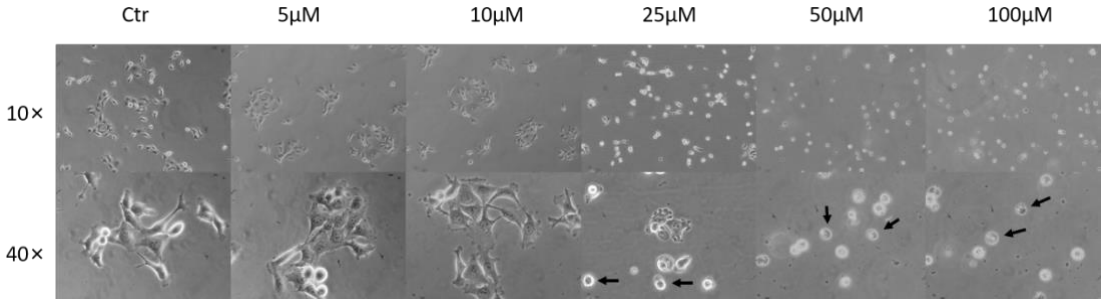

Fig.6. Effect of NPS-2143 on cell morphology and apoptotic formation in C4-1 cells. The black arrows indicate the formation of apoptotic bodies, chromatin condensation, cell shrinkage, and bleb formation. These results are representative of one of three similar experiments, and the pictures were magnified at 10 × and 40 ×.

2.1.3 NPS-2143 significantly induce apoptosis in C4-1 cells after incubation 24 hours

Subsequently, I confirmed apoptosis in C4-1 cells through dual staining utilizing the Chromatin Condensation/Dead Cell Apoptosis Kit. AO emits green fluorescence when bound to double-stranded DNA (dsDNA) and red fluorescence when bound to single-stranded DNA (ssDNA) or RNA, while EB intercalates into DNA and emits red fluorescence when bound. Live cells exhibited a uniform green fluorescence（Fig.7 white arrow）. Early apoptotic cells displayed green staining accompanied by bright green dots within the nuclei, indicative of chromatin condensation and nuclear fragmentation (Fig.7 red arrow). Late apoptotic cells incorporating ethidium bromide exhibited an orange stain. Notably, late apoptotic cells displayed condensed and frequently fragmented nuclei, distinguishing them from necrotic cells, which also stained orange（Fig.7, blue arrow）. However, the nuclear morphology of necrotic cells resembled that of viable cells, lacking condensed chromatin.

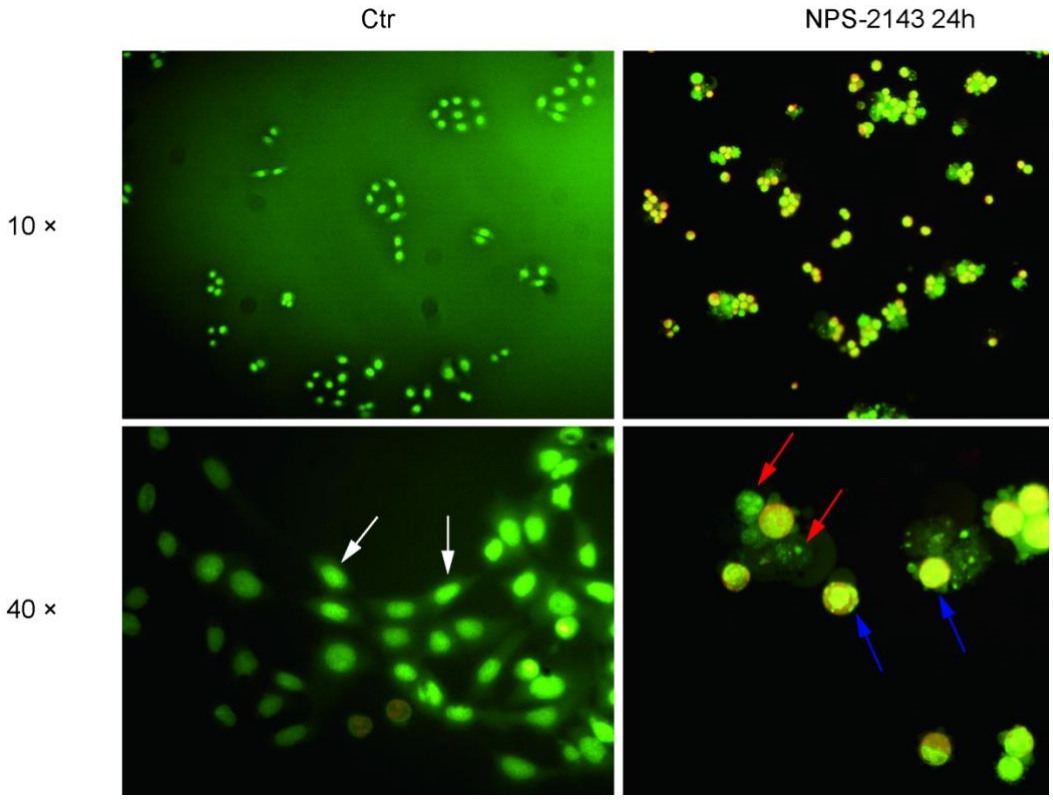

Fig.7. Double-staining with the Chromatin Condensation/Dead Cell Apoptosis Kit following a 24-hour treatment of C4-1 cells with NPS-2143. Live cells will appear uniformly green（white arrow）. Early apoptotic cells will stain green and contain bright green dots in the nuclei due to chromatin condensation and nuclear fragmentation (red arrow). Late apoptotic cells will also incorporate ethidium bromide and, therefore, stain orange（blue arrow）.

2.1.4 Executioner caspase-3 activity

Caspase-3 is a key executioner caspase that plays a central role in the intracellular (intrinsic) apoptosis pathway. In my experiment, the level of caspase-3 enzymatic activity at basal was between 18 and 24 after being in the Ctr group. However, a significant surge in caspase-3 activity was evident after 18 hours of the NPS-2143 treatment, when a 6.2-fold increase appeared with respect to the control group. This increment did not persist in the 24-hour NPS-2143 treated group, where caspase-3 levels were 1.9 folds higher than those in the control group. This phenomenon is likely attributable to apoptotic occurrences, leading to a reduction in surviving C4-1 cells and subsequent attenuation of caspase-3 activation(Fig.8).

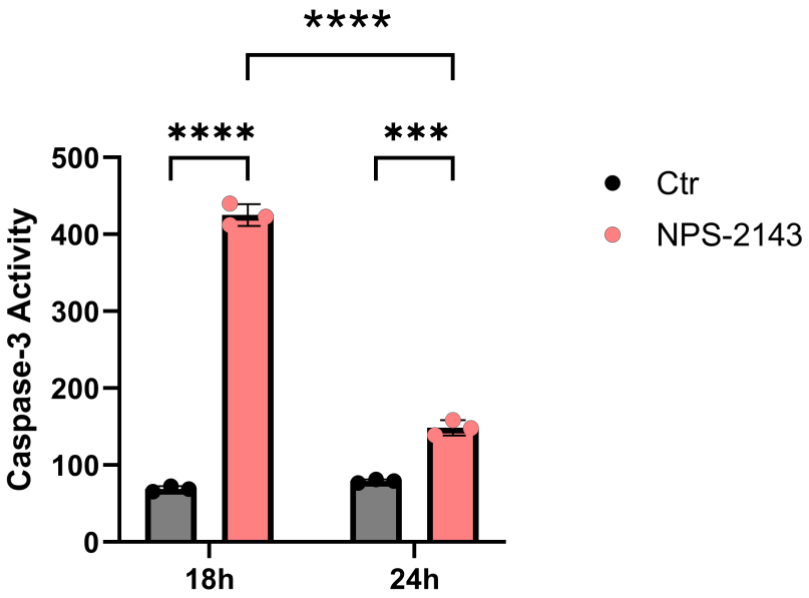

Fig.8. Caspase-3 integral intensity enzymatic activity at 18 and 24 hours after NPS-2143 treatment. Means ± SD (n=3). ***p < 0.0005, ****p < 0.0001.

2.2 Calhex 231 inhibited C4-1 cell proliferation and promoted apoptosis

2.2.1 The viability of C4-1 cells is significantly inhibited by Calhex 231

It is known that at low concentrations, Calhex 231 acts as PAM activity, while at higher concentrations, action as NAM activity[51]. Specifically, Calhex 231 concentrations in the 5-25 μM range exhibited a NAM effect and modulated apoptosis within 3 hours. In Comparison, NPS-2143 required a time span of 24 hours to achieve a similar effect. Moreover, the IC_{50} value of Calhex 231 for C4-1 cell viability was determined to be 17.53 μM. Employing the standard curve for Relative Celltiter Blue Fluorescence of C4-1 cells (Fig.6.A), the count of viable cells in the 5μM, 10μM, and 25μM groups were 23,367, 15,757, and 3,772, respectively. Correspondingly, the apoptosis rates of C4-1 cells stood at 24.1%, 49.11%, and 87.8%, respectively (Fig.9).

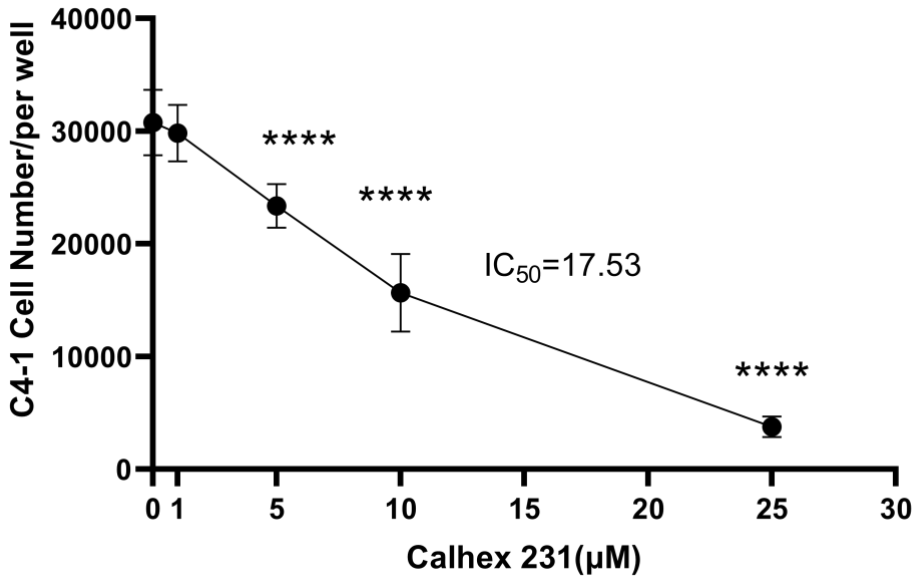

Fig.9. The impact of Calhex 231 3-hour treatment on C4-1 cell viability was assessed using Cell titer Blue Assay. Viability of C4-1 cells with different concentrations of Calhex 231. (****P < 0.0001).

2.2.2 Cell morphology following 3-hours treatment with Calhex 231

I observed the morphological changes in C4-1 cells treated with Calhex 231 under the microscope. The morphology of C4-1 cells exhibited apoptotic features after 3 hours. Notably, the Calhex 231 at one μM concentration did not significantly deviate from the control. However, concentrations of 5 μM, 10 μM, and 25 μM of Calhex 231 elicited evident apoptosis. The emergence of apoptotic bodies, chromatin condensation, cell shrinkage, and bleb formation were conspicuous and demarcated by black arrows (Fig. 10).

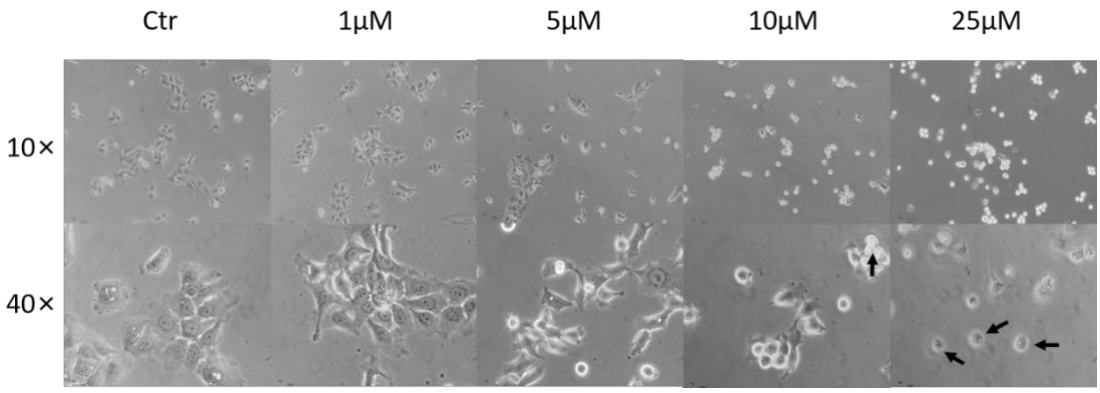

Fig.10. The effect of Calhex 231 on cell morphology and apoptotic formation in C4-1 cells was investigated. The formation of apoptotic bodies, chromatin condensation, cell shrinkage, and bleb formation were observed (indicated by black arrows). The data presented is representative of one of three similar experiments. The pictures were magnified at 10 × and 40 ×.

2.2.3 Calhex 231 significantly induces apoptosis in C4-1 cells after incubation 3-hours

Apoptosis in C4-1 cells was affirmed through double staining with a chromatin condensation/dead cell apoptosis kit. Cells were exposed to Calhex 231 at a concentration of 17μM for 3 hours (Fig.11). Vital cells exhibit homogeneous green fluorescence (white arrows). Early apoptotic cells showcase green staining with prominent green dots in the nucleus, signifying chromatin condensation and nuclear fragmentation (red arrows). Late apoptotic cells, supplemented with ethidium bromide, demonstrate orange staining, with condensed and frequently fragmented nuclei distinguishing them from necrotic cells, which are similarly stained orange (blue arrows).

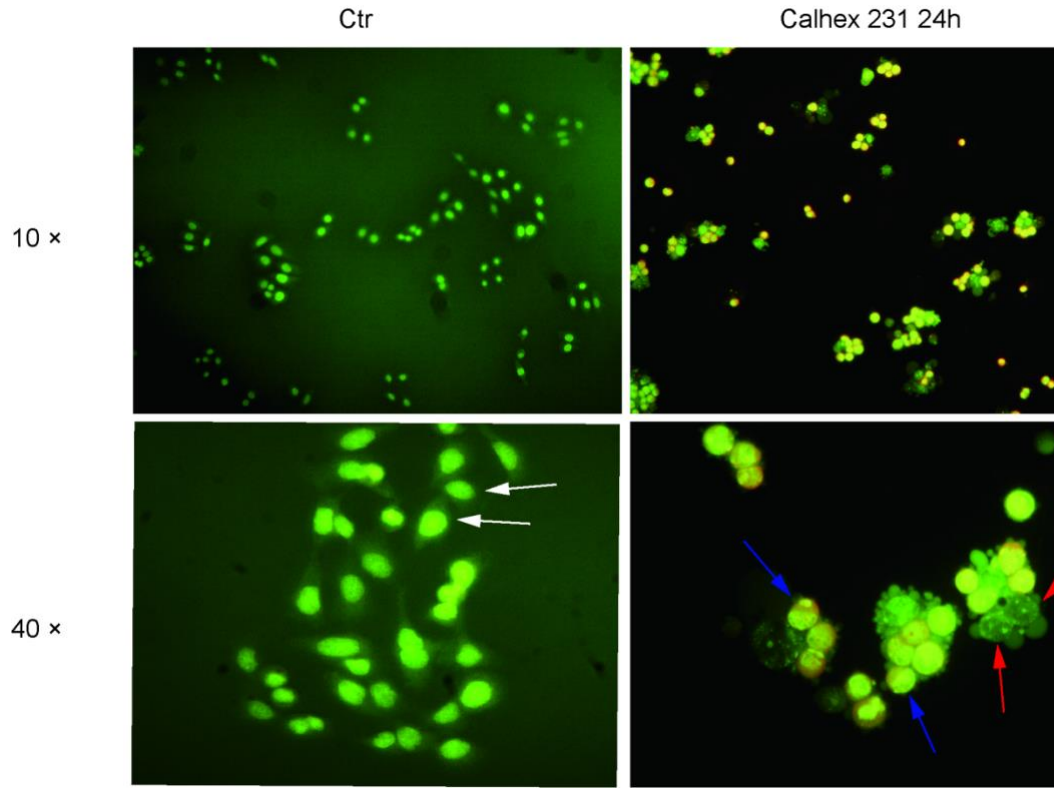

Fig.11. Following double-staining with the Chromatin Condensation/Dead Cell Apoptosis Kit. Green fluorescence is uniformly displayed by vital cells (white arrows). Early apoptotic cells will stain green and contain bright green dots in the nuclei due to chromatin condensation and nuclear fragmentation(red arrow). Late apoptotic cells will also incorporate ethidium bromide and, therefore, stain orange（blue arrow）.

3.Gd^{3+} promoted proliferation in C4-1 cells

Gd^{3+} was one agonist of calcium-sensing receptor; I checked the effect of Gd^{3+} on the proliferation of C4-1 cells, adding it at four different concentrations to the culture medium. The C4-1 cell proliferation was evaluated by Celltiter Blue Assay as described in the experimental section in Fig.12. The increase of cell viability was observed at concentrations of 100 μM Gd^{3+} at 24h. This result is similar to that of Ying Zhang et al., who reported that Gd at a concentration of less than 100 μM promotes proliferation by inducing HeLa cells to enter S phase[52]. The result indicated that Gd^{3+} promoted proliferation in C4-1 cells.

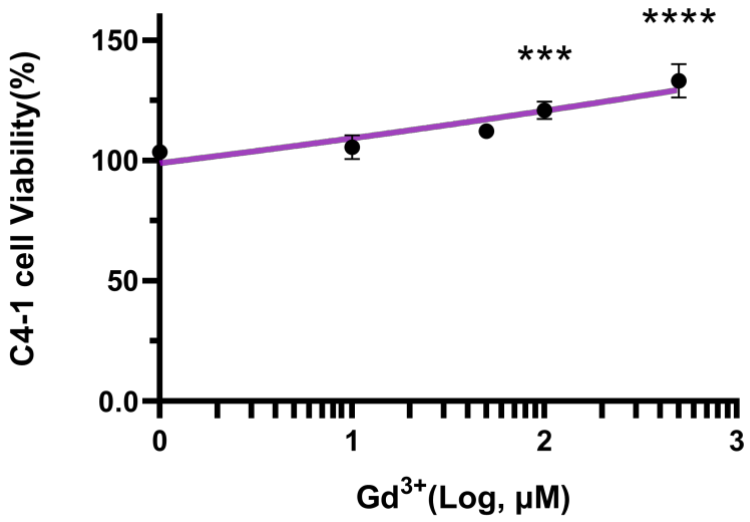

Fig.12. Effects of Gd^{3+} on C4-1 cell proliferation by Alamar blue assay. Various concentrations of Gd were added to the medium and incubated for 24h respectively. Data were presented as means ± SD(n=3; ***P＜0.001, ****P＜0.0001)

4. NPS-2143 significantly inhibits CaSR expression in cervical cancer C4-1 cell line

Demonstrated that CaSR is expressed in various types of cervical cancer cell lines. The C4-1 cell line, which contains human papillomavirus type 18 (HPV-18) DNA sequences and expresses HPV-18 RNA, was included in the study. After adding NPS-2143 35μM, western blotting was performed to detect the expression of CaSR at 6, 18, and 24 hours. The results showed a slight increase in CaSR expression at 6 hours, but there was no statistical difference with Ctr. However, the expression level significantly decreased at 18 and 24 hours after the action of NPS-2143 (Fig.13).

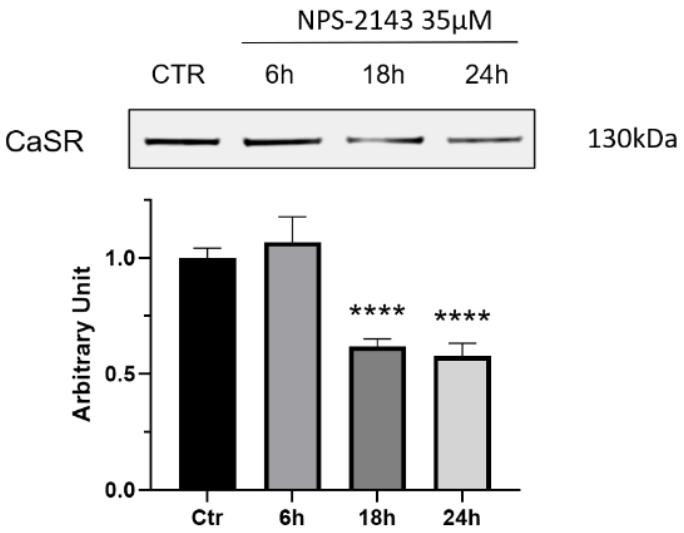

Fig.13. The expression level of CaSR was decreased in C4-1 cells after treatment with NPS-2143(arbitrary units normalized to CaSR protein expression). The protein expression level of CaSR in C4-1 cells was determined by western blot and quantification of CaSR protein expression level. Means ± SD (n=3). **p < 0.0001 vs. Ctr.

5. The C4-1 cell line exhibits high expression of HPV-related proteins E6 and E7, which can be inhibited by NPS-2143

E6 and E7 are biomarkers of cervical cancer cells and drive cancer progression. Therefore, therapies targeting E6 and E7 have been shown to be effective in removing abnormally proliferating malignant cells. E6 and E7 were highly expressed in the C4-1 cell line; after the addition of 35μM NPS-2143, the expression was reduced at six h, 18h, and 24h compared with the control group, and the levels were significantly decreased (Fig.14). The results showed that NPS-2143 could significantly inhibit the expression of E6, E7 in C4-1 cell line.

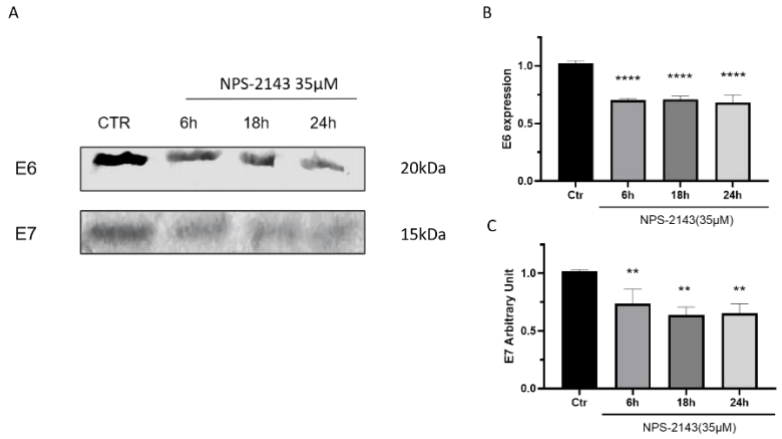

Fig.14. Effect of NPS-2143 on the expression of E6, E7. A) Western blot analysis of the expression levels of E6 and E7 proteins in C4-1 cells treated with NPS-2143(35μM) at 6, 18hour and 24 hours. **B, C)** Quantification of expression levels of E6, E7. Means ± SD (n=3). ****P＜0.0001, **P＜0.001.

6. Expression of cell cycle proteins

The effect of NPS-2143 on the levels of some proteins involved in cell cycle progression was accessed employing Western blot. Whole-cell lysates were prepared after 24 hours of NPS-2143 treatment, and the expression levels of cyclin D1, B1, and E were analyzed. Twenty-four hours reduced the expression of cyclin D1, B1, and E compared to controls (Fig.15). These results suggest that NPS-2143 down-regulates the expression of specific cell cycle proteins, potentially leading to cell cycle arrest and, ultimately, growth inhibition.

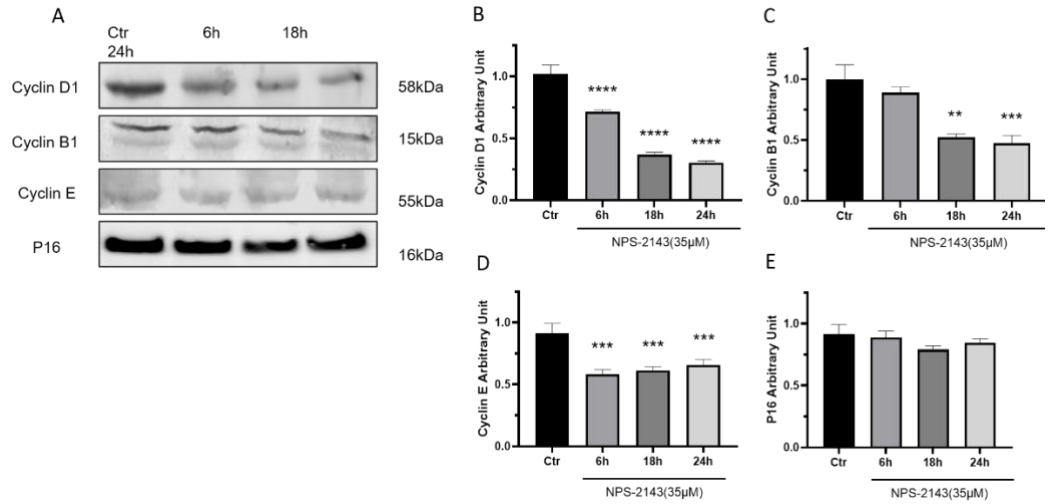

Fig.15. Cell cycle protein expression in C4-1 cells by different concentrations of NPS-2143. A) Cell lysates were analyzed by western blotting using specific antibodies to cyclin D1 and B1. **B-**

E) Quantification of Cyclin D1, Cyclin B1, and Cyclin E Means expression levels. Means ± SD (n=3). **p < 0.001, ***p < 0.0005, ****p < 0.0001 vs. control.

7. Impact of NPS-2143 on dsDNA expression

DNA replication occurs during the S phase. C4-1 cells were cultured in DMEM supplemented with 5% FBS and showed proliferation, as demonstrated by a progressive increase in double-stranded DNA (dsDNA) expression. Instead, when C4-1 was treated with NPS-2143, a marginal, albeit statistically insignificant, rise in dsDNA was noted after 8 hours of incubation, while noteworthy disparities in dsDNA emerged at 18, 24, and 48 hours of incubation (**P < 0.001, ***P < 0.0005, ****P < 0.0001, respectively). Correspondingly, there was a respective 1.93-fold, 2.35-fold, and 3.78-fold elevation in dsDNA levels. Conversely, treatment with NPS-2143 resulted in a substantial reduction in the dsDNA content of untreated C4-1 (P < 0.05) at the 24-hour and 48-hour intervals (Fig.16.A). Upon comparative analysis across distinct time points, no statistically significant difference was evident between the control and NPS-2143-treated cohorts after 8 hours of incubation. However, a pronounced diminution in dsDNA was observed in the NPS-2143-treated cohort (*P < 0.005, ****P < 0.0001, ****P < 0.0001) at 18, 24, and 48 hours, respectively, compared to the corresponding time points in the control group, representing reductions of 49%, 79%, and 87% (Fig.16.B).

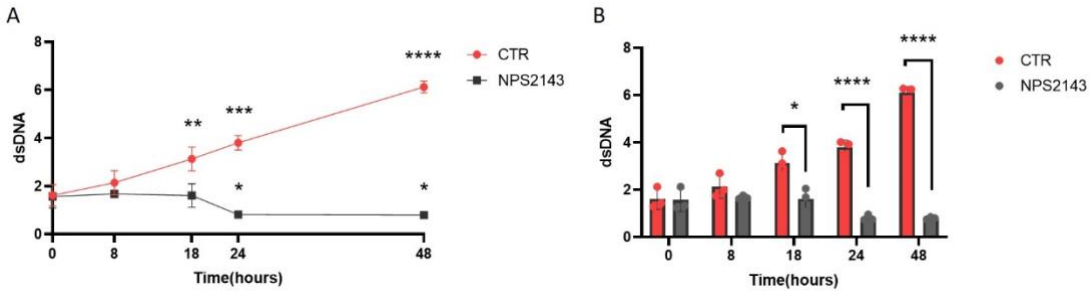

Fig.16. Changes in dsDNA level in C4-1 cells. A) Comparison within groups, dsDNA increased significantly in the control group at 18, 24, and 48 hours. Conversely, dsDNA decreased significantly in the NPS-2143 groups at 24 and 48 hours, respectively. B. Comparison between groups, dsDNA expression between the control and NPS-2143 groups at 18, 24, and 48 hours of incubation were statistically different. Means ± SD (n=3). (*P < 0.005, **P < 0.001, ***P < 0.0005,

****P < 0.0001).

8. The effect of NPS-2143 on the Human Apoptosis signaling Pathway utilizing a protein array

The Human Apoptosis Signaling Pathway Array Kit is a rapid, sensitive, and economical tool for simultaneously detecting the relative levels of phosphorylated or cleaved 19 Apoptosis pathway proteins. Figure 17 displays arrays of membranes (one membrane per group) covering the entire range of ordinary human apoptotic pathways tested, including AKT(P-Ser473), ATM(P-Ser1981), ERK1/2(P-T202/Y204), JNK(P-Thr183/Tyr185), and TAK1(P-Ser412) signaling pathways(Fig.17). It is evident that AKT(P-Ser473), ATM(P-Ser1981), JNK(P-Thr183/Tyr185), and TAK1(P-Ser412) apoptotic signaling pathways were significantly reduced. The phosphoprotein kinases were most significantly reduced were AKT(P-Ser473), ATM(P-Ser1981), and TAK1(P-Ser412), with reductions of 69.751%, 39.852%, and 47.211% at 90min after treating with NPS-2143, respectively(Fig.18). These results demonstrate influenced the level of phosphorylation of some kinases that were involved in the phosphorylation on apoptosis.

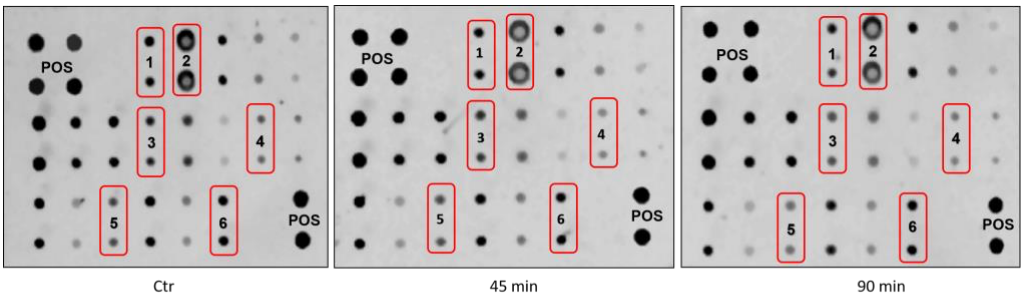

Fig.17. The Human Apoptosis Signaling Pathway Array Kit is used to simultaneously detect the relative levels of phosphorylated or cleaved 19 apoptosis pathway proteins（each array made of 2 different membranes）. The red rectangles include the duplicate dots of the predominant apoptotic pathway 1-6. Means ± SD (n=3).

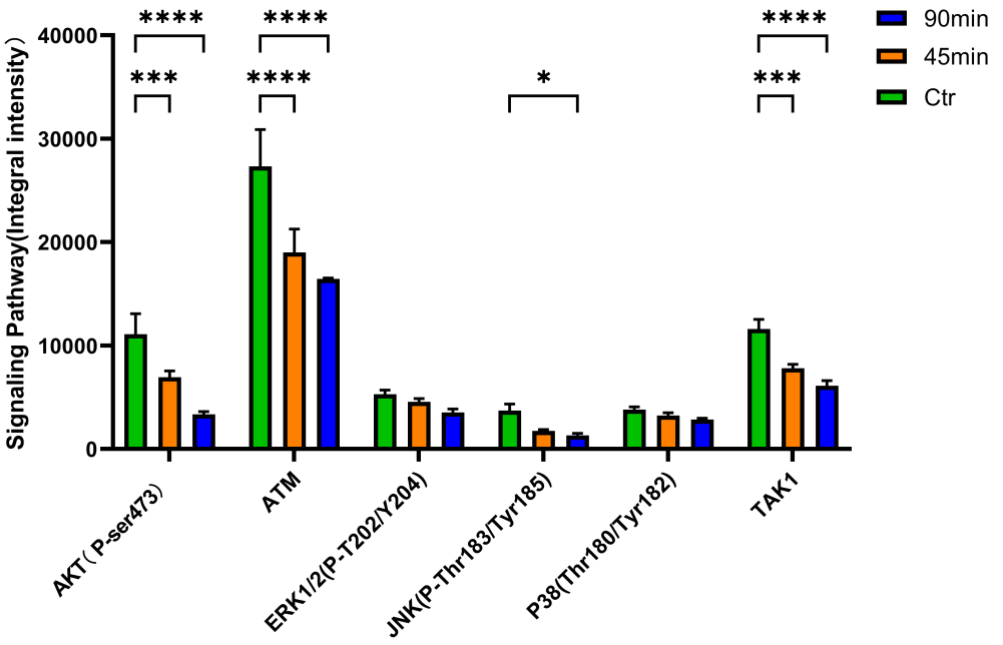

Fig.18. The integral intensity of proteins detected by apoptosis in signaling pathways assays after 45 and 90 minutes of treatment in the Control group and NPS-2143 groups. The AKT(P-Ser473), ATM(P-Ser1981), ERK1/2(P-T202/Y204), JNK(P-Thr183/Tyr185), and TAK1(P-Ser412) signaling pathways showed significant differences when compared with the Control group. Means ± SD (n=3). (*P < 0.005, **P < 0.001, ***P < 0.0005, ****P < 0.0001).

9. Ly294002 inhibit PI3K by Alamar Blue assay

To ascertain the role of the PI3K/Akt activity on cell proliferation and apoptosis in the C4-1 cell line, we employed the inhibitor LY294002. The standard curve was shown in Fig.19.A. Relative to the control group, the 25, 50, and 75 μM LY294002 treated C4-1 cells exhibited significant reductions in cell viability analyzed using cell Celltiter Blue^{TM} Assay ($p < 0.0001$), decreasing by 68.3%, 80.02%, and 83.63%, respectively (Fig.19.B). Similarly, after 24 hours of cell proliferation using a cell counter, the control group proliferated and increased the cell number from 30,000 to 44,210. Following 24 hours of cell proliferation in the control group, the average cell count reached 44,210. This represented a 1.43-fold increase compared to the initial inoculation of 30,000 cells 24 hours prior. Conversely, upon treatment with Ly294002 at 25, 50, and 75 μM

concentrations for the same duration, cell numbers diminished by an average of 30,084, 35,350, 27,015, and 36,979, respectively (Fig.19.C). After a 24-hour treatment period, in the Ly294002-treated groups. Apoptotic bodies, chromatin condensation, cell shrinkage, and bleb formation were evident. (Fig.19.D)

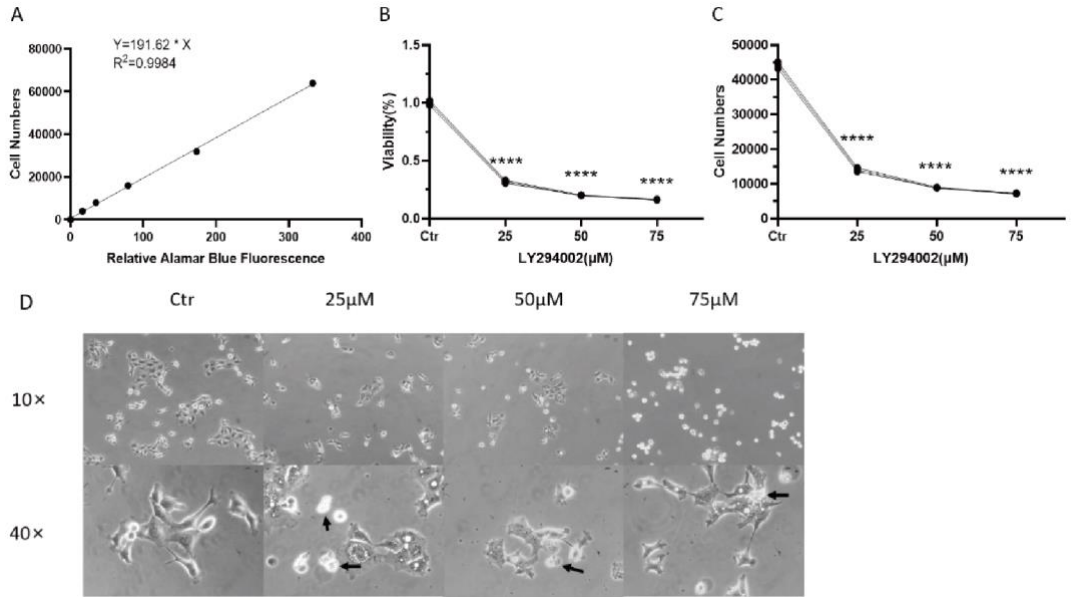

Fig.19. The effect of LY294002 on cell viability, cell number, and cell morphology at varying concentrations. A) The standard curve for C4-1 cells was measured using Celltiter Blue™ Assay. **B)** The cell viability of the C4-1 cell line was measured after treatment with 25, 50, and 75 μM Ly294002 for 24 hours. **C)** Using celltiter blue the number of cells was calculated based on the standard curve(see page 20, Fig.5.A). **D)** The formation of apoptotic bodies, chromatin condensation, cell shrinkage, and bleb formation were visible(indicated by black arrows). The data presented is representative of one of three similar experiments. Means ± SD(n=3), ****$p < 0.0001$ vs. Ctr. The pictures were magnified 10 × and 40 ×.

10. The CaMKII inhibition by KN-93 was determined

KN-93 is a selective inhibitor of calmodulin-dependent protein kinase II (CaMKII), acting by competitively blocking its calmodulin-binding site to prevent activation. The impact of KN-93 on cell proliferation and apoptosis in the C4-1 cell line was investigated using Celltiter Blue Assay. The standard curve is shown in Fig.20.A. Cells were exposed to varying concentrations of KN-93 in culture media for 24 hours. A notable dose-dependent decline in cell proliferation was observed. Relative to the control group, the

5, 10, 20, and 40 μM KN-93-treated groups exhibited significant reductions in C4-1 cell viability, with decreases of 30.60%, 47.17%, 62.10%, and 72.16%, respectively ($p < 0.0001$) (Fig.20.B). Initially, 30,000 C4-1 cells were seeded and evenly dispersed in a 12-well plate. Following 24 hours of proliferation in the control group, the average cell count reached 43,933. However, upon treatment with KN-93 at concentrations of 5, 10, 20, and 40 μM for the same duration, cell numbers decreased by an average of 13,785, 20,743, 27,015, and 31,243, respectively (Fig.20.C). Apoptotic bodies, chromatin condensation, cell shrinkage, and bleb development were clearly visible. (Fig.20.D)

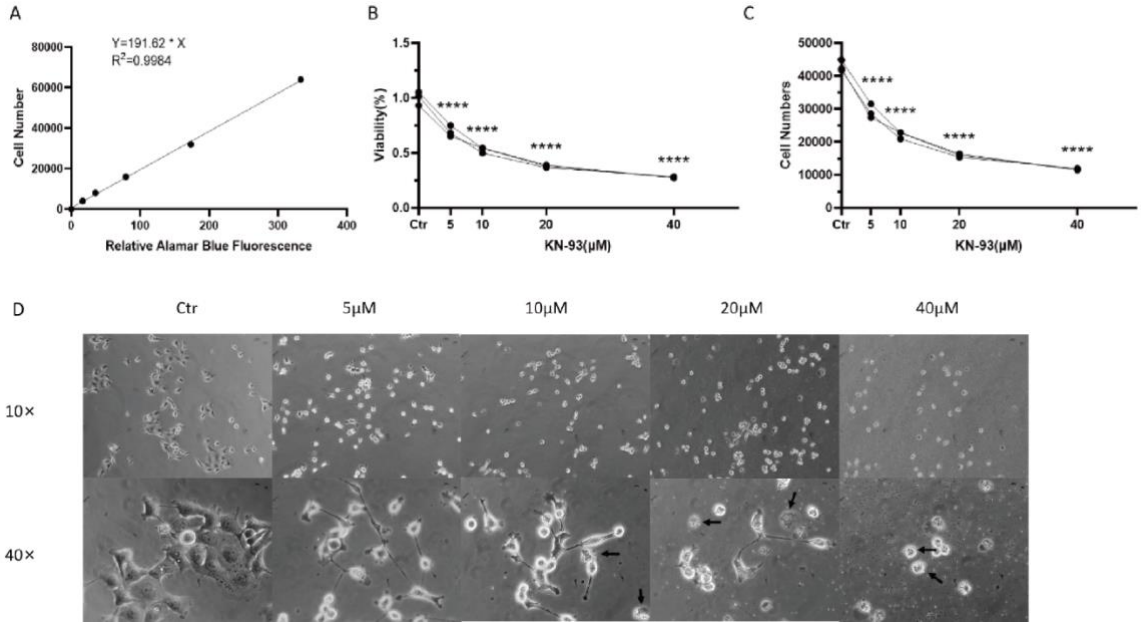

Fig.20. The impact of KN-93 on Celltiter Blue Assay cell viability, cell number, and morphology at varying concentrations was investigated. A) The standard curve for C4-1 cells was measured using Celltiter Blue™ Assay. B) The cell viability of the C4-1 cell line was measured after treatment with 5, 10, 20, and 40 μM KN-93 for 24 hours. C) The cell number was calculated based on the standard curve(See Fig). The results were compared with the control group, and statistical analysis showed a significant difference (****P<0.0001). D) The formation of apoptotic bodies, chromatin condensation, cell shrinkage, and bleb formation were visible (indicated by black arrows). The data presented is representative of one of three similar experiments. Means ± SD(n=3), ****$p < 0.0001$ vs. Ctr. The pictures were magnified at 10 x and 40 x.

11. Torin-1 causes C4-1 cell apoptosis by inhibiting the mTOR signaling pathway

Torin-1, a potent small molecule inhibitor targeting mTOR kinase, has been demonstrated to play a critical regulator of cellular processes such as protein synthesis, growth, metabolism, and autophagy[53]. Compared to the control group in our experiment, C4-1 cell proliferation markedly increased after 24 hours in the absence of Torin-1 (0 μM group, P<0.0001), as well as in the 0.005μM and 0.01μM groups. Higher doses of Torin-1 effectively restrained C4-1 cell proliferation, with the 0.05μM group showing sustained inhibition. The increase of Torin-1 concentrations (1μM, 2μM, and 4μM) notably enhanced tumor cell apoptosis (Fig.21).

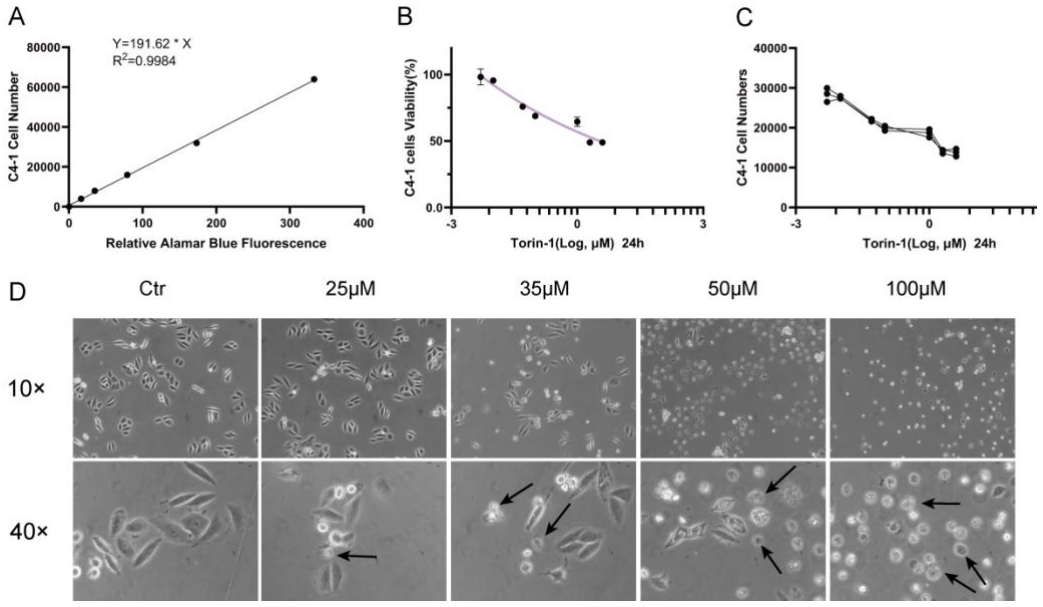

Fig.21. The effect of Torin-1 on cell viability, cell number, and cell morphology at varying concentrations. A) The standard curve for C4-1 cells was measured using Celltiter Blue™ Assay. **B)** The cell viability of the C4-1 cell line was measured after treatment with 0.005, 0.01, 0.05, 0.1, 1, 2, 4 μM Torin-1 for 24 hours. **C)** The number of cells was calculated based on the standard curve and Compared to the control group. **D)** The formation of apoptotic bodies, chromatin condensation, cell shrinkage, and bleb formation were visible (indicated by black arrows). The data presented is representative

of one of three similar experiments. Means ± SD(n=3), ****p < 0.0001 vs. Ctr. The pictures were magnified at 10 x and 40 x.

12. Effect of NPS-2143 on Siha cells

Siha cells were seeded at various densities ranging from 2,000 to 64,000 cells per well in 12-well plates. Upon cell adhesion, Celltiter Blue reagent was used to construct a standard curve (Fig.22.A). Subsequently, Siha cells were plated in 12-well plates, and different concentrations of NPS-2143 were administered to the Siha cells. After 24 hours, the growth of the control and treated groups was analyzed using Celltiter Blue. Noteworthy inhibition of cell proliferation was observed in the treatment the NPS-2143 concentration exceeded 35 μM (P < 0.0001). Moreover, a progressive decline in Siha cell viability was evident at NPS-2143 concentrations of 50 μM and 100 μM (Fig.22.B). NPS-2143-treated groups (35 μM, 50 μM, and 100 μM) showed a substantial decrease in cell numbers, with average cell counts of 28,049, 13,435, and 707, respectively. Correspondingly, the average cell count in the control group was 35,238 (Fig.22.C). Black arrows identified prominent morphological alterations, including the formation of apoptotic bodies, chromatin condensation, cell shrinkage, and bleb formation. (Fig.22.D)

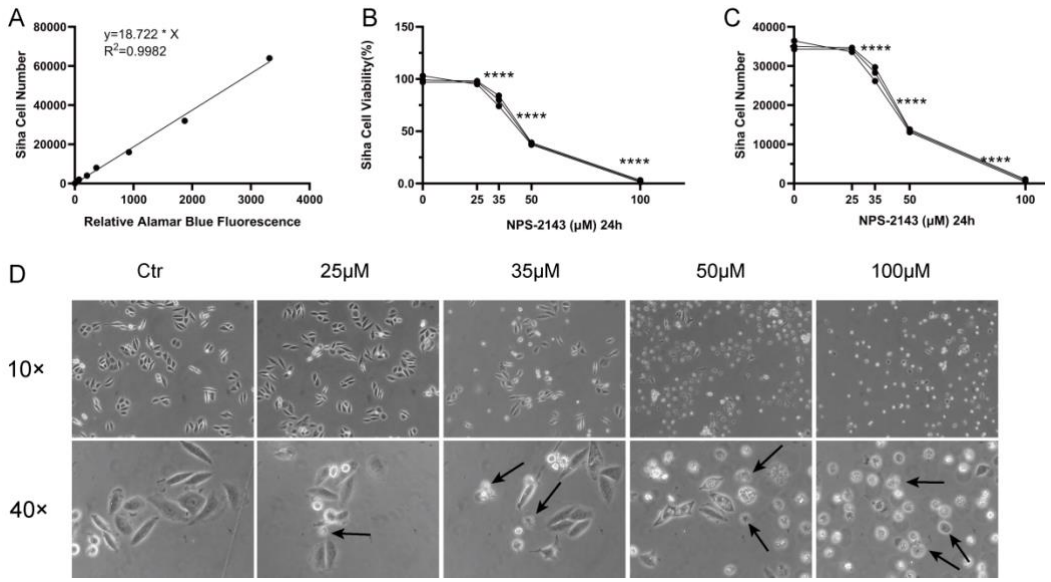

Fig.22. The impact of NPS-2143 on the proliferation, apoptosis, and morphology of Siha cells. A) Siha cell proliferation was evaluated by quantifying the relative Celltiter Blue fluorescence intensity across varying cell counts. **B)** Following exposure to distinct NPS-2143 concentrations for 24 hours, Siha cell viability was assessed via Celltiter Blue Assay. **C)** A decrease in Siha cell numbers/wells after 24-hour treatment with different NPS-2143 concentrations was analyzed. **D)** The formation of apoptotic bodies, chromatin condensation, cell shrinkage, and bleb formation were visible and indicated by black arrows. The data presented is representative of one of three similar experiments. Means ± SD(n=3), ****$p < 0.0001$ vs. Ctr. The pictures were magnified at 10 x and 40 x.

13. Effect of NPS-2143 on C33A cells

Initially, C33A cells were seeded in 12-well plates at different densities ranging from 4,000 to 64,000 cells per well. Following cell adhesion, Celltiter Blue Assay was made to establish a standard curve (Fig.23.A). Subsequently, C33A cells were cultured in 12-well plates, and different concentrations of NPS-2143 were administered to C33A cells. After 24 hours, the growth of the control and NPS-2143-treated groups. Notable inhibition of cell proliferation was observed in the NPS-2143-treated groups. A significant increase in apoptosis in C33A cells ($P < 0.0001$) was noted at NPS concentrations of 35 μM, 50 μM, and 100 μM, respectively (Fig.23.B). C33A cell viability decreased by 37.27%, 91.93%, and 95.90%, respectively. Cell counting was performed using Celltiter Blue Assay. In the treatment groups with NPS-2143 concentrations of 35 μM, 50 μM, and 100 μM, a Significant reduction in cell number was observed, with mean cell counts decreasing by 12,869, 31,736, and 33,099, respectively (Fig.23.C). The visible morphological features, including apoptotic bodies, chromatin condensation, cell shrinkage, and bleb formation, were marked by black arrows. (Fig.23.D)

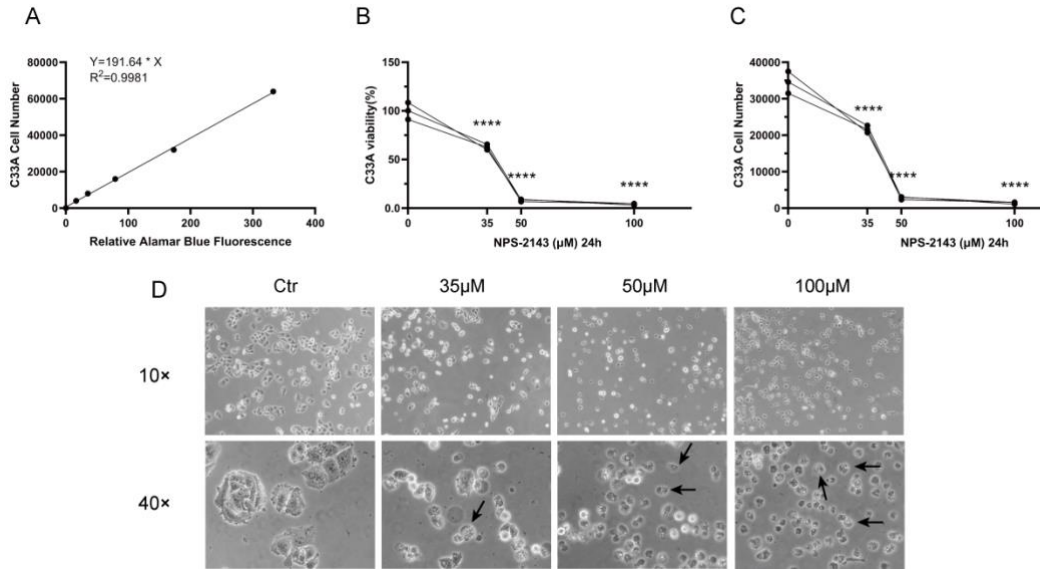

Fig.23. The effect of different concentrations of NPS-2143 on C33A cell proliferation and apoptosis. A) C33A cell numbers were assessed by Celltiter Alamar Assay, and standard curves were constructed. **B)** C33A viability was assessed by the relative Celltiter Alamar Assay fluorescence intensity after exposure to different concentrations of NPS-2143 for 24 h. **C)** Changes in C33A numbers per well analyzed after 24 h treatment with different concentrations of NPS-2143. **D)** The formation of apoptotic bodies, chromatin condensation, cell shrinkage, and bleb formation were visible and indicated by black arrows. The data presented is representative of one of three similar experiments. Means ± SD(n=3), ****$p < 0.0001$ vs. Ctr. The pictures were magnified at 10 x and 40 x.

14. Effect of NPS-2143 on HaCaT cells

Subsequent investigation delved into the impact of NPS-2143 on the HaCaT cell line, which had been seeded in 12-well plates at densities ranging from 8,000 to 64,000 per well. Following cell adhesion, Celltiter Alamar Assay was performed to establish a standard curve (Fig.24.A). Then, HaCaT cells were cultured in 12-well plates and

exposed to different concentrations of NPS-2143 (35 μM, 50 μM, and 100 μM). The treatment with NPS-2143 induced a notable reduction in the cellular viability of HaCaT cells after 24 hours ($P < 0.0001$) (Fig.24.B). Specifically, HaCaT cell activity decreased by 39.33%, 81.67%, and 98.67%. A significant decrease in cell numbers was evident in the NPS-2143-treated groups. The average number of cells was reduced by 17,627, 35,449, and 43,240 cells, respectively (Fig.24.C). Apoptotic bodies, chromatin condensation, cell shrinkage, and bleb formation were distinctly observed, as indicated by black arrows, highlighting key morphological changes. (Fig.24.D)

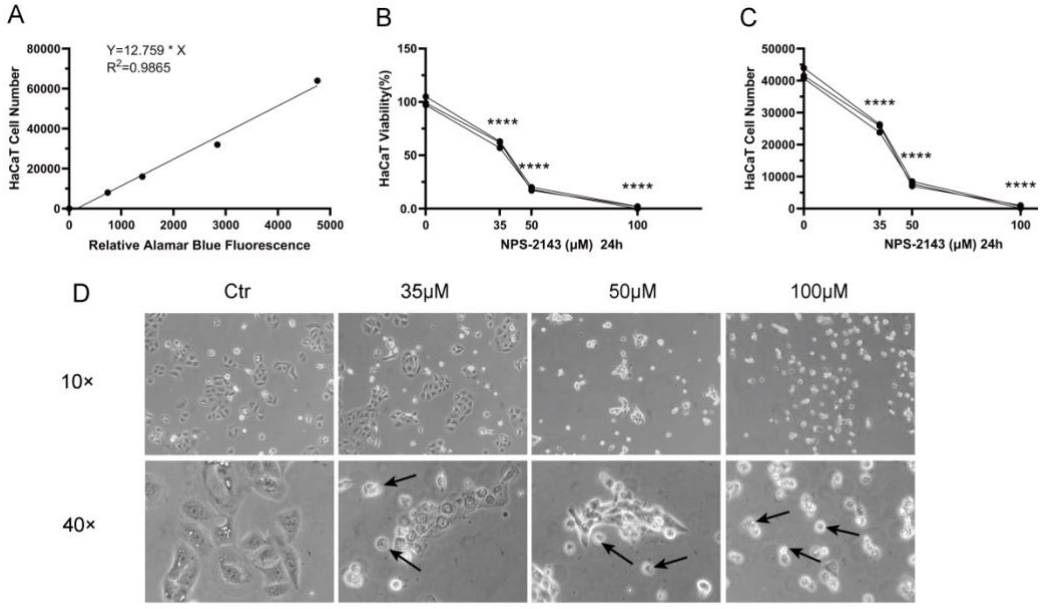

Fig.24. The impact of different concentrations of NPS-2143 on HaCaT cell proliferation and apoptosis. **A)** HaCaT cell numbers were evaluated through Celltiter Blue Assay for standard curves. **B)** HaCaT cell viability was assessed after 24-hour exposure to different concentrations of NPS-2143. **C)** A decrease in HaCaT cell number was examined after 24 hours of treatment with diverse concentrations of NPS-2143. **D)** The formation of apoptotic bodies, chromatin condensation, cell shrinkage, and bleb formation were visible and indicated by black arrows. Revealing statistically significant changes. Means ± SD(n=3), ****$p < 0.0001$ vs. Ctr. The pictures were magnified at 10 x and 40 x.

Discussion

Cervical cancer remains one of the most prevalent malignancies affecting women globally, with a significant proportion of cases linked to high-risk human papillomavirus (HPV) infection[54,55]. While current treatments, including surgery, chemotherapy, and radiotherapy, have improved patient outcomes, resistance to these therapies and disease recurrence remain significant challenges. This underscores the urgent need for novel therapeutic targets and strategies[56,57]. In recent years, the calcium-sensing receptor (CaSR), a G protein-coupled receptor that regulates calcium homeostasis and signaling, has emerged as a potential target in cancer therapy due to its involvement in tumorigenesis, metastasis, and cell survival. Calcilytics, such as NPS-2143 and Calhex 231, are small-molecule antagonists of CaSR that have shown promise in preclinical studies for their ability to disrupt CaSR-mediated signaling, thereby inducing apoptosis and inhibiting proliferation in cancer cells[58]. Furthermore, in HPV-positive cervical cancer, viral oncoproteins E6 and E7 play a pivotal role in disrupting normal cell cycle regulation and apoptosis. Understanding how CaSR antagonism affects these oncoproteins and their downstream effects on cellular signaling pathways could provide critical insights into the development of targeted therapies[59]. This study builds on this foundation by investigating the effects of CaSR antagonists, specifically NPS-2143 and Calhex 231, on cervical cancer cell lines. Additionally, the study examines the interplay between CaSR signaling, HPV oncoproteins, and cell cycle regulation, offering a comprehensive analysis of the therapeutic potential of targeting CaSR in cervical cancer.

1.CaSR Expression and Its Role in Cervical Cancer Cells

The results of this study revealed significant expression of the calcium-sensing receptor (CaSR) across various cervical cancer cell lines (C4-1, SiHa, C33A) and HaCaT

cells, with notably higher expression levels observed in SiHa and C33A cells compared to C4-1 cells. This differential expression pattern highlights the potential heterogeneity of CaSR regulation among cervical cancer subtypes. The overexpression observed in cervical cancer cells suggests that CaSR may be implicated in cervical carcinogenesis, a hypothesis that remains underexplored in current literature. CaSR is gaining recognition for its contributions to tumor biology, influencing critical processes such as cell proliferation, apoptosis, migration, and invasion[60]. Findings in other malignancies suggest that CaSR may serve as a crucial molecular hub linking calcium signaling with oncogenic pathways[61]. However, the precise implications of CaSR expression in cervical cancer remain unclear. Notably, CaSR expression was observed in SiHa, C33A, and C4-1 cells. C4-1 cells harbor the HPV-18 genome, SiHa cells contain an integrated HPV-16 genome, and C33A cells are derived from an HPV-negative cervical cancer. HaCaT cells, originating from normal adult skin, represent spontaneously transformed keratinocytes cultured in vitro. This suggests that CaSR is involved in both HPV-related and HPV-independent carcinogenesis mechanisms, with its expression in HPV-negative cervical cancer and keratinocytes reflecting its broad regulatory role in epithelial cell and cancer cell survival, consistent with previous findings[62]. Given that C4-1 cells harbor HPV-18, a major etiological agent of cervical cancer, subsequent studies in this research will focus on C4-1 cells, further investigating the potential role of CaSR in HPV-driven carcinogenesis.

2. Inhibition of Cell Proliferation and Induction of Apoptosis by CaSR Antagonists

The present study highlights the potent anti-proliferative and pro-apoptotic effects of the CaSR antagonist NPS-2143 on C4-1 cervical cancer cells, offering valuable insights into the therapeutic potential of targeting CaSR in cervical cancer[63]. By disrupting cell viability and inducing programmed cell death, NPS-2143 demonstrates the multifaceted mechanisms through which CaSR antagonists may alter tumor cell

behavior, thereby positioning itself as a candidate for further exploration in cancer therapy[64]. NPS-2143 significantly inhibited C4-1 cell proliferation in a dose-dependent manner, with an IC50 value of 35.25 μM. This observation aligns with existing research suggesting that cancer cells exhibit heightened sensitivity to pharmacological inhibition of CaSR[65,66]. Notably, significant reductions in cell viability were observed at concentrations of 25 μM and above, while lower concentrations (5 μM and 10 μM) had minimal effects. These findings suggest a critical threshold of CaSR antagonism required to disrupt the cellular proliferation machinery effectively. Such a threshold may reflect the degree to which CaSR-mediated signaling pathways must be inhibited to alter downstream oncogenic mechanisms. At higher concentrations (25 μM, 50 μM, 100 μM), NPS-2143-treated C4-1 cells displayed hallmark morphological changes associated with apoptosis. These changes included nuclear condensation, chromatin fragmentation, cell shrinkage, and apoptotic body formation—features consistent with programmed cell death rather than necrosis. This morphological evidence underscores the specificity of NPS-2143 in activating apoptosis pathways. In contrast, cells treated with lower concentrations (5 μM and 10 μM) retained their normal morphology, further reinforcing the dose-dependent nature of the observed effects. Such morphological changes are critical indicators of cellular response to therapeutic agents and provide a visual confirmation of apoptosis induction.

The apoptotic effects of NPS-2143 were further validated through chromatin condensation and nuclear fragmentation assays. Dual staining using chromatin-specific dyes revealed an increase in both early and late apoptotic cells. Early apoptotic cells exhibited chromatin condensation and nuclear fragmentation, while late apoptotic cells displayed condensed and fragmented nuclei with distinct staining patterns. Importantly, necrotic cells, characterized by a lack of chromatin condensation, were clearly differentiated from apoptotic populations. These findings demonstrate the precision of NPS-2143 in steering cells toward regulated apoptosis, thereby minimizing the risk of nonspecific cytotoxicity associated with necrosis.

Further mechanistic insights were gained by examining caspase-3 activity, a critical executioner enzyme in the intrinsic apoptosis pathway[67]. A significant increase in

caspase-3 activity was observed 18 hours post-treatment, with levels rising approximately 6.2-fold compared to the control group. This sharp increase highlights the central role of caspase-3 in orchestrating the downstream events of apoptosis. However, at 24 hours, caspase-3 activity decreased to 1.9-fold above baseline levels. This attenuation may be attributed to a reduction in the population of viable cells due to extensive apoptosis or to the temporal regulation of caspase activation during the apoptotic process [68]. These results emphasize the dynamic nature of apoptosis and the importance of time-dependent analyses in understanding the effects of therapeutic agents.

Interestingly, a comparison with another CaSR antagonist, Calhex 231, revealed distinct temporal dynamics in apoptosis induction[69]. While NPS-2143 required 24 hours to exert its full apoptotic effect, Calhex 231 induced apoptosis within 3 hours of treatment. This difference suggests that NPS-2143 may act through slower but potentially more sustained engagement with CaSR or associated signaling pathways. Conversely, the rapid effects of Calhex 231 imply an immediate disruption of cellular processes, potentially through alternative mechanisms or pathways. These variations underscore the complexity of CaSR signaling in cancer cells and highlight the potential for distinct therapeutic applications depending on the pharmacokinetic and pharmacodynamic profiles of the antagonists. The ability of NPS-2143 to inhibit cell proliferation and induce apoptosis through targeted modulation of CaSR positions it as a promising candidate for cervical cancer therapy.

3. The Effect of Gd^{3+} on Cell Proliferation

The findings from this study reveal that Gd^{3+}, a known calcium-sensing receptor (CaSR) agonist, promotes the proliferation of C4-1 cervical cancer cells in a dose-dependent manner, adding complexity to our understanding of the role of calcium signaling in cancer cell behavior and highlighting the dualistic nature of CaSR modulation in tumor progression[70]. Gadolinium (Gd^{3+}) is a lanthanide metal ion recognized for its pharmacological action as a CaSR agonist[30]. In the current study, I

evaluated the impact of Gd^{3+} on C4-1 cell proliferation by adding varying concentrations of Gd^{3+} (up to 100 μM) to the culture medium and assessing cell viability through the Celltiter Blue assay. The results demonstrated a significant increase in cell viability at 100 μM Gd^{3+} after 24 hours, suggesting that Gd^{3+} promotes cell proliferation. This observation aligns with findings from Ying Zhang et al., who reported that Gd^{3+} at similar concentrations induces S-phase entry and enhances survival in HeLa cervical carcinoma cells. These parallel findings provide strong evidence of Gd^{3+}' s ability to stimulate cancer cell proliferation through its interaction with CaSR.

The ability of Gd^{3+} to enhance C4-1 cell proliferation underscores the critical yet complex role of CaSR and calcium signaling in cancer biology. The activation of CaSR by agonists like Gd^{3+} can lead to calcium influx, activating downstream signaling pathways such as MAPK/ERK, PI3K/AKT, and NF-κB, which are well-documented in promoting tumor cell growth and survival[25,71]. In contrast, CaSR antagonists like NPS-2143 were shown in this study to induce apoptosis and inhibit proliferation, demonstrating the dualistic nature of CaSR modulation. This duality highlights that the role of CaSR in cancer is highly context-dependent, influenced by factors such as the cellular environment, the type of ligand (agonist or antagonist), and the downstream signaling pathways activated[72]. The finding that Gd^{3+} promotes C4-1 cell proliferation raises important questions about the context-specific actions of CaSR and its ligands. While the pro-apoptotic effects of CaSR antagonists suggest their potential as therapeutic agents, the pro-proliferative effect of Gd^{3+} suggests that CaSR activation may contribute to tumor progression in certain settings. This paradox reflects the broader complexity of calcium signaling in cancer, where both hyperactivation and inhibition can yield context-dependent outcomes. In the case of Gd^{3+}, the observed proliferation could be linked to its ability to modulate intracellular calcium levels, thereby enhancing cell cycle progression. Specifically, the increase in S-phase entry reported suggests that Gd^{3+} may promote the expression of cell cycle regulators such as cyclins and cyclin-dependent kinases (CDKs). Additionally, the interaction of Gd^{3+} with other calcium channels or receptors cannot be excluded and warrants further investigation.

These findings have important implications for the development of CaSR-targeted therapies in cervical cancer. While CaSR antagonists like NPS-2143 have shown promise in inhibiting tumor growth and inducing apoptosis, the potential for CaSR agonists like Gd^{3+} to enhance proliferation highlights the need for careful consideration of the therapeutic context. For example, in tumors with high CaSR expression, targeting CaSR with antagonists might yield better therapeutic outcomes, whereas in tumors with altered downstream calcium signaling, alternative strategies may be required. Therefore, future research should focus on elucidating the molecular mechanisms underlying Gd^{3+}-induced proliferation, particularly the signaling pathways activated downstream of CaSR. Additionally, studies should explore the interplay between CaSR and other calcium-regulated pathways to identify potential points of therapeutic intervention. Comparative analyses of CaSR modulation in different cervical cancer cell lines, such as HeLa and C4-1, could further clarify the context-dependent roles of CaSR agonists and antagonists. The dualistic effects of CaSR modulation on cervical cancer cells highlight the complexity of calcium signaling in tumor biology. While Gd^{3+} promotes C4-1 cell proliferation through CaSR activation, the contrasting effects of antagonists like NPS-2143 underscore the need for a nuanced approach to targeting calcium signaling in cancer therapy. These findings pave the way for future studies aimed at developing more effective and context-specific therapeutic strategies.

4. Inhibition of CaSR and HPV Oncogenes by NPS-2143 in C4-1 Cervical Cancer Cells

We observed the significant inhibitory effect of the CaSR antagonist NPS-2143 on the expression of CaSR and HPV-related proteins E6 and E7 in the C4-1 cervical cancer cell line. The C4-1 cell line, which contains human papillomavirus type 18 (HPV-18) DNA sequences and expresses HPV-18 RNA, serves as a relevant model for studying the molecular mechanisms underlying cervical cancer progression, especially in HPV-associated carcinogenesis. The results showed that NPS-2143, when applied at a

concentration of 35 μM, led to a significant decrease in CaSR expression after 18 and 24 hours, further supporting the role of CaSR as a modulator of cellular processes in cervical cancer. At 6 hours, a slight increase in CaSR expression was observed, but this did not reach statistical significance, suggesting that the effects of NPS-2143 on CaSR expression may be time-dependent and require prolonged exposure to achieve significant modulation.

In cervical cancer, the dysregulation of CaSR and its downstream signaling pathways may contribute to tumorigenesis and resistance to therapy. By inhibiting CaSR expression, NPS-2143 may disrupt these crucial pathways, thereby reducing the growth and survival of cancer cells. The time-dependent reduction in CaSR expression observed with NPS-2143 treatment suggests that prolonged inhibition of CaSR may be necessary to exert significant anticancer effects. This aligns with the known role of CaSR in regulating cellular processes such as proliferation and apoptosis, which could be dysregulated in cancer cells. Therefore, targeting CaSR with NPS-2143 could offer a novel therapeutic approach for cervical cancer treatment, particularly in HPV-associated cancers where CaSR signaling may play a critical role.

In addition to inhibiting CaSR expression, NPS-2143 also significantly reduced the expression of the HPV-related oncogenes E6 and E7 in C4-1 cells. E6 and E7 are critical drivers of cervical carcinogenesis, as they promote the degradation of tumor suppressor proteins such as p53 and retinoblastoma protein (Rb), allowing for uncontrolled cell proliferation and evasion of apoptosis. The downregulation of E6 and E7 expression upon NPS-2143 treatment further underscores the potential of targeting CaSR as a means to modulate key oncogenic pathways in HPV-related cancers[73]. Notably, the significant reduction of E6 and E7 expression at multiple time points (6, 18, and 24 hours) suggests that NPS-2143 may exert its effects on cervical cancer cells by modulating the expression of these crucial oncogenes, thus inhibiting the abnormal cell cycle progression driven by HPV.

The inhibitory effects of NPS-2143 on both CaSR and HPV-related proteins highlight its potential as a therapeutic agent in cervical cancer. Previous studies have shown that targeting HPV oncogenes, particularly E6 and E7, can lead to the regression

of cervical tumors and the restoration of normal cellular functions[74]. By simultaneously inhibiting CaSR expression and reducing the levels of E6 and E7, NPS-2143 may provide a dual mechanism of action, effectively targeting both the aberrant calcium signaling pathways and the HPV-driven oncogenic pathways that drive cervical cancer progression. Given the high expression of HPV-related proteins in cervical cancer and the established role of CaSR in regulating various signaling pathways, these findings suggest that NPS-2143 could be a promising candidate for future clinical studies aimed at treating HPV-associated cancers.

The combined effects of NPS-2143 on both CaSR and E6/E7 expression emphasize the importance of understanding the interplay between calcium signaling and HPV oncogenesis[75]. This study provides novel insights into the potential for CaSR antagonists to modulate both the calcium-mediated signaling networks and the viral oncoproteins critical for cervical cancer progression. Further investigations are needed to elucidate the precise molecular mechanisms through which NPS-2143 inhibits the expression of these key proteins and to evaluate its therapeutic efficacy in vivo.

5. Modulation of HPV-Related Proteins and Cell Cycle Regulation

The present study also explores the impact of NPS-2143 on the expression of key proteins involved in cell cycle regulation, particularly cyclins D1, B1, and E, and its effects on DNA replication, as evidenced by alterations in double-stranded DNA (dsDNA) levels. The findings demonstrate that NPS-2143 down-regulates the expression of these cell cycle proteins after 24 hours of treatment, suggesting a disruption of cell cycle progression that may contribute to the observed growth inhibition. Cyclins are critical regulators of the cell cycle, and their down-regulation often leads to cell cycle arrest, which is consistent with the induction of apoptosis in C4-1 cells[76,77]. The reduction in cyclin D1, B1, and E levels may reflect interference with the transition through specific cell cycle checkpoints, especially the G1/S and G2/M phases, further implicating NPS-2143 as a potent modulator of cell cycle progression in cervical cancer

cells.

Furthermore, our data indicate that NPS-2143 treatment significantly affected dsDNA expression, which is a direct marker of DNA replication in the S phase. A gradual increase in dsDNA levels was observed in control C4-1 cells, indicating ongoing proliferation, while treatment with NPS-2143 resulted in a notable increase in dsDNA expression at 18, 24, and 48 hours. This rise in dsDNA levels initially suggests an attempt at DNA replication; however, the significant reductions in dsDNA content at these time points may indicate a subsequent inhibition of DNA synthesis or a blockade in the cell cycle that prevents proper replication. Specifically, at 24 and 48 hours, NPS-2143 treatment led to a 79% and 87% reduction in dsDNA levels, respectively, which could be attributed to a blockade in the S phase or a premature induction of apoptosis, effectively halting cell cycle progression.

These results are consistent with prior studies showing that manipulation of cell cycle regulators, particularly in HPV-positive cancer cells, can restore normal cell cycle checkpoints and trigger apoptosis. In cervical cancer, HPV E6 and E7 proteins are essential for maintaining the malignant phenotype by inactivating tumor suppressors like p53 and Rb, thereby promoting unchecked cell cycle progression[78]. In this study, NPS-2143 was found to significantly inhibit the expression of these HPV-related proteins in C4-1 cells, potentially restoring normal cell cycle regulation. The suppression of E6 and E7 could be a critical mechanism through which NPS-2143 induces apoptosis, as these oncoproteins are responsible for evading apoptosis and maintaining cell immortality. Thus, the combined effects of CaSR antagonism on both the regulation of cell cycle proteins and the inhibition of HPV oncogenes might explain the enhanced therapeutic potential of NPS-2143 in treating HPV-related cancers, such as cervical carcinoma.

6.Impact on PI3K/AKT/mTOR Signaling Pathway

The results from the Human Apoptosis Signaling Pathway Array Kit clearly illustrate that NPS-2143, a CaSR antagonist, exerts a profound effect on various critical

apoptotic signaling pathways, particularly the PI3K/AKT/mTOR pathway[79]. By targeting multiple signaling proteins involved in cell survival, our data indicate that NPS-2143 significantly down-regulates the phosphorylation of key kinases, including AKT (P-Ser473), ATM (P-Ser1981), JNK (P-Thr183/Tyr185), and TAK1 (P-Ser412). These findings suggest that NPS-2143 disrupts the activation of pro-survival pathways that are crucial for maintaining cancer cell proliferation and resistance to apoptosis. The most notable reductions in phosphorylation were observed in AKT, ATM, and TAK1, with decreases of 69.75%, 39.85%, and 47.21%, respectively, within 90 minutes of treatment. These results are consistent with the role of these kinases in regulating apoptosis, and their inhibition underscores the potential of CaSR antagonism as a strategy to enhance apoptotic cell death in cervical cancer cells.

The PI3K/AKT/mTOR signaling pathway is widely recognized as a central regulator of cell survival, proliferation, and resistance to chemotherapy in many cancers[80,81]. This Pathway is frequently over-activated in cancer cells, leading to enhanced survival and tumor progression. In our study, we further explored the relationship between CaSR antagonism and this Pathway by using the PI3K inhibitor LY294002 and the mTOR inhibitor Torin-1. Both inhibitors significantly reduced the viability of C4-1 cells and promoted apoptosis, reinforcing the hypothesis that CaSR signaling modulates the PI3K/AKT/mTOR pathway in cervical cancer cells. The inhibitory effects of LY294002 and Torin-1 are consistent with the well-established role of PI3K/AKT/mTOR signaling in maintaining cellular homeostasis and promoting resistance to cell death. In this context, NPS-2143 may disrupt this Pathway by interfering with upstream signaling events, leading to the inhibition of downstream survival signals.

Furthermore, the observed reduction in the phosphorylation of key apoptotic proteins suggests that NPS-2143 not only targets the PI3K/AKT/mTOR axis but also affects other related survival pathways, such as the ATM/ATR and JNK pathways. The ATM kinase is involved in DNA damage response and cell cycle regulation[82], while JNK signaling is implicated in stress-induced apoptosis[83]. The down-regulation of these pathways by NPS-2143 supports the idea that CaSR antagonism might alter the balance

between survival and death signals within cancer cells, promoting apoptotic cell death.

Given the complex interplay of these pathways, the data suggest that CaSR antagonism could serve as an effective strategy to sensitize cancer cells to apoptosis, particularly in HPV-related cancers where survival pathways like PI3K/AKT/mTOR are often upregulated. Combining CaSR antagonists with other inhibitors targeting the PI3K/AKT/mTOR pathway could offer a more potent therapeutic approach, exploiting synergistic effects to overcome resistance and enhance treatment efficacy.

7. Inhibition of PI3K by LY294002 in C4-1 Cervical Cancer Cells

The results of the study demonstrate that LY294002, a potent inhibitor of PI3K, significantly reduces cell viability and induces apoptosis in the C4-1 cervical cancer cell line. In this investigation, we observed a dose-dependent decrease in cell proliferation and viability with increasing concentrations of LY294002 (25 μM, 50 μM, and 75 μM). Specifically, cell viability decreased by 68.3%, 80.02%, and 83.63%, respectively, in Comparison to the control group. This inhibition of cell proliferation was further corroborated by cell count data, which revealed a marked reduction in the number of viable cells in LY294002-treated groups compared to controls. After 24 hours of incubation, the control group exhibited a 1.43-fold increase in cell number, from 30,000 to 44,210, whereas the LY294002-treated groups showed diminished cell counts, with average reductions of approximately 30,084, 35,350, and 36,979 at concentrations of 25, 50, and 75 μM, respectively.

The observed reduction in cell number and viability suggests that LY294002 effectively inhibits the PI3K/Akt signaling pathway, a critical regulator of cell survival and proliferation. By inhibiting PI3K, LY294002 likely disrupts these processes, leading to a cessation of cell division and triggering apoptotic pathways. Notably, the morphological changes observed in LY294002-treated cells, such as chromatin condensation, cell shrinkage, and bleb formation, are characteristic features of apoptosis. These findings suggest that the reduction in cell viability is not merely due to cell cycle

arrest but also to the induction of programmed cell death[84].

The induction of apoptosis following PI3K inhibition further highlights the central role of the PI3K/Akt pathway in the survival of cervical cancer cells. This Pathway is known to promote cellular survival and resist apoptotic signals through various mechanisms, including the phosphorylation and activation of downstream targets such as Akt, which in turn regulates processes such as cell cycle progression and inhibition of pro-apoptotic factors[85]. By targeting this Pathway, LY294002 not only halts cell proliferation but also reprograms the cellular response to stress, ultimately leading to cell death. This underscores the potential therapeutic value of PI3K inhibitors, particularly in cancers driven by aberrant PI3K signaling. Moreover, the observed dose-dependent effects in this study suggest that LY294002 can be optimized for therapeutic use, as higher concentrations yield more pronounced reductions in cell viability and increased apoptotic markers. These findings also align with previous studies demonstrating the anticancer properties of PI3K inhibitors in various tumor models[86]. However, the ability of LY294002 to induce apoptosis in the C4-1 cell line also indicates that the effect is not solely dependent on the inhibition of cell proliferation but involves the engagement of multiple apoptotic pathways, potentially enhancing its overall efficacy as a therapeutic agent. Our results provide strong evidence that LY294002, by inhibiting the PI3K/Akt signaling pathway, effectively reduces the viability of C4-1 cervical cancer cells and induces apoptosis. These findings support the potential of PI3K inhibitors as part of targeted therapeutic strategies in cervical cancer and other malignancies with PI3K pathway dysregulation. Future studies should explore the molecular mechanisms underlying this effect and evaluate the in vivo efficacy of LY294002 in preclinical models to further establish its potential as a treatment option for cervical cancer.

8. Impact of KN-93 on C4-1 Cell Proliferation and Apoptosis

The observed decline in cell proliferation following treatment with KN-93 in the C4-1 cervical cancer cell line highlights the significant role of CaMKII in regulating cell

survival. CaMKII is a multifunctional kinase involved in various cellular processes, including cell cycle progression, differentiation, and apoptosis[87,88]. By inhibiting CaMKII with KN-93, a marked reduction in cell viability was noted across all concentrations, suggesting that CaMKII activity is crucial for maintaining cell proliferation in these cancer cells. The dose-dependent effects seen in this study, with reductions in cell viability reaching up to 72.16% at 40 μM KN-93, further underscore the therapeutic potential of CaMKII inhibition in cervical cancer.

Notably, these results align with previous studies indicating that CaMKII is a key player in tumor progression, including its involvement in regulating key pathways that influence cell survival. This supports the hypothesis that inhibiting CaMKII can disrupt cancer cell proliferation and induce apoptosis, particularly in the context of human papillomavirus (HPV)-related cancers. Given that the C4-1 cell line expresses high levels of HPV-18 and CaMKII is known to interact with various signaling cascades, such as the PI3K/Akt pathway, this study adds to the growing evidence that targeting CaMKII could disrupt the survival mechanisms of HPV-related cancer cells.

In terms of apoptosis, KN-93 treatment led to the characteristic hallmarks of programmed cell death, including chromatin condensation, cell shrinkage, and bleb formation[89]. These morphological changes are indicative of apoptosis rather than necrosis, further suggesting that KN-93 may trigger intrinsic apoptotic pathways. The dose-dependent induction of apoptosis observed in this study further supports the idea that CaMKII inhibition is an effective strategy for inducing cancer cell death. The extent of cell number reduction following KN-93 treatment also implies that prolonged exposure to this inhibitor leads to significant cell cycle disruption, further preventing cancer cell growth.

Additionally, KN-93's effects on cell viability and apoptosis highlight the potential for its use in combination with other therapeutic agents targeting survival pathways, such as PI3K/Akt or mTOR inhibitors. The combination of these therapies may lead to a more comprehensive treatment strategy, targeting multiple key regulatory pathways that contribute to tumorigenesis and resistance to conventional therapies[90]. These findings also emphasize the importance of CaMKII in the broader landscape of cancer therapy.

Given that CaMKII is involved in several crucial signaling pathways, including those related to cell survival, apoptosis, and metastasis, its inhibition may serve as a novel therapeutic approach to treat cervical cancer, especially in HPV-positive cases. Future studies should explore the molecular mechanisms by which CaMKII inhibition leads to apoptosis and whether these effects are synergistic with other targeted therapies.

9. Broader Implications for Therapy and Future Directions

Our findings highlight the potential of CaSR antagonism as a novel therapeutic approach for cervical cancer, particularly in HPV-positive tumors. The ability of NPS-2143 and Calhex 231 to induce apoptosis via the PI3K/AKT/mTOR signaling pathway suggests that these agents could be valuable in combination therapies. Furthermore, the modulation of HPV E6/E7 expression and cell cycle proteins provides an additional rationale for targeting CaSR in the treatment of HPV-associated cancers. However, several questions remain to be addressed. For instance, the differential responses observed in different cervical cancer cell lines (C4-1, SiHa, C33A) and HaCaT cells warrant further investigation into the molecular determinants of sensitivity to CaSR antagonism. Additionally, in vivo studies are needed to validate the therapeutic efficacy of CaSR antagonists in preclinical models of cervical cancer.

Conclusion

This study provides a comprehensive analysis of the role of the calcium-sensing receptor (CaSR) in cervical cancer cells, shedding light on its functional significance and potential therapeutic implications. CaSR expression was found to be elevated across multiple cervical cancer cell lines (C4-1, SiHa, C33A) as well as in HaCaT cells, suggesting a heterogeneous regulation of CaSR across different cervical cancer subtypes and normal epithelial cells.

The use of CaSR antagonists, NPS-2143 and Calhex 231, revealed significant anti-proliferative and pro-apoptotic effects on C4-1 cells. NPS-2143 inhibited cell proliferation in a dose-dependent manner, with an IC50 of 35.25 μM, and induced classic apoptotic morphological changes, enhanced caspase-3 activity, and altered apoptotic signaling pathways. In contrast, Calhex 231 induced apoptosis more rapidly within 3 hours, highlighting distinct temporal dynamics in response to different CaSR antagonists. These findings underscore the potential of CaSR antagonists as promising therapeutic agents for cervical cancer. Moreover, the CaSR agonist Gd^{3+} stimulated C4-1 cell proliferation, emphasizing the dual role of CaSR modulation in tumor progression. The context-dependent effects of CaSR ligands underscore the need for careful consideration when designing CaSR-targeted therapies.

NPS-2143 not only suppressed CaSR expression but also significantly reduced the levels of HPV-associated oncogenes E6 and E7 in C4-1 cells. This dual inhibition of aberrant calcium signaling and HPV-driven oncogenesis presents a potential therapeutic approach targeting both pathways in HPV-associated cervical cancers.

Regarding cell cycle regulation, NPS-2143 downregulated key cell cycle proteins, including cyclins D1, B1, and E, and impaired dsDNA expression, indicating a blockade in cell cycle progression, likely through S-phase arrest or the induction of premature apoptosis.

Furthermore, NPS-2143 significantly modulated the PI3K/AKT/mTOR signaling pathway, reducing the phosphorylation of key kinases. This, in conjunction with the effects of the PI3K inhibitor LY294002 and mTOR inhibitor Torin-1, highlights the critical role of this Pathway in mediating the pro-apoptotic effects of CaSR antagonism.

In conclusion, this study establishes CaSR as a crucial regulator of cell proliferation and apoptosis in cervical cancer, acting through the PI3K/AKT/mTOR signaling axis. The inhibition of CaSR by NPS-2143 and Calhex 231 holds considerable therapeutic promise, particularly for HPV-positive cervical cancers. However, further studies are required to elucidate the molecular mechanisms, assess cell line-specific sensitivities, and validate the efficacy of CaSR antagonists in in vivo models. These efforts will pave the way for the clinical translation of CaSR-targeted therapies in the treatment of cervical

cancer.

References

1. LaVigne AW, Triedman SA, Randall TC, et al. Cervical cancer in low and middle income countries: addressing barriers to radiotherapy delivery. *Gynecol Oncol Rep*. 2017;22:16-20.

2. Cohen PA, Jhingran A, Oaknin A, et al. Cervical cancer. *The Lancet*. 2019;393(10167):169-182. doi:10.1016/S0140-6736(18)32470-X

3. Tewari KS. Cervical cancer. *N Engl J Med*. 2025;392(1):56-71.

4. Tan LF, Rajagopal M, Selvaraja M. An Overview on the Pathogenesis of Cervical Cancer. *Curr Trends Biotechnol Pharm*. 2023;17(1):717-734.

5. Munger K, White EA. What are the essential determinants of human papillomavirus carcinogenesis? *Mbio*. 2024;15(11):e00462-24.

6. Serrano B, Brotons M, Bosch FX, et al. Epidemiology and burden of HPV-related disease. *Best Pract Res Clin Obstet Gynaecol*. 2018;47:14-26.

7. Peng Q, Wang L, Zuo L, et al. HPV E6/E7: insights into their regulatory role and mechanism in signaling pathways in HPV-associated tumor. *Cancer Gene Ther*. 2024;31(1):9-17.

8. Janiszewska J, Kostrzewska-Poczekaj M, Wierzbicka M, Brenner J, et al. HPV-driven oncogenesis—much more than the E6 and E7 oncoproteins. *J Appl Genet*. Published online 2024:1-9.

9. Araldi R P, Sant'Ana T A, Módolo D G, et al. The human papillomavirus (HPV)-related cancer biology: An overview[J]. Biomedicine & pharmacotherapy, 2018, 106: 1537-1556.

10. Doorbar J, Egawa N, Griffin H, Kranjec C, Murakami I. Human papillomavirus molecular biology and disease association. *Rev Med Virol*. 2015;25:2-23.

11. Rector A, Van Ranst M. Animal papillomaviruses. *Virology*. 2013;445(1-2):213-223.

12. Cho EH, Park MS, Woo HY, et al. Evaluation of clinical usefulness of HPV-16 and HPV-18 genotyping for cervical cancer screening. *J Gynecol Oncol*. 2024;35(6):e72.

13. Mahendra INB, Budiana ING, Putra IGM, Mulyana RS, Winata IGS, Harjoto BS. E6/E7 Oncogenes Mutation of Human Papillomavirus Type 16 Associated with P16 Protein Expression in Cervical Cancer. *Eur J Med Health Sci*. 2023;5(2):81-84.

14. Estêvão D, Costa NR, da Costa RMG, et al. Hallmarks of HPV carcinogenesis: The role of E6, E7 and E5 oncoproteins in cellular malignancy. *Biochim Biophys Acta BBA-Gene Regul Mech*. 2019;1862(2):153-162.

15. Bieging KT, Mello SS, Attardi LD. Unravelling mechanisms of p53-mediated tumour suppression. *Nat Rev Cancer*. 2014;14(5):359-370.

16. Thomas M, Banks L. Human papillomavirus (HPV) E6 interactions with Bak are conserved amongst E6 proteins from high and low risk HPV types. *J Gen Virol*. 1999;80(6):1513-1517.

17. Thomas M, Banks L. Inhibition of Bak-induced apoptosis by HPV-18 E6. *Oncogene*. 1998;17(23):2943-2954.

18. Huang J, Yin C, Wang J. Relationship between vaginal microecological changes and oncogene E6/E7 and high-risk human papillomavirus infection. *J Obstet Gynaecol*. 2023;43(1):2161349.

19. Yu L, Majerciak V, Lobanov A, et al. HPV oncogenes expressed from only one of multiple integrated HPV DNA copies drive clonal cell expansion in cervical cancer. *Mbio*. 2024;15(5):e00729-24.

20. Lo Cigno I, Calati F, Girone C, et al. High-risk HPV oncoproteins E6 and E7 and their interplay with the innate immune response: Uncovering mechanisms of immune evasion and therapeutic prospects. *J Med Virol*. 2024;96(6):e29685.

21. Magno AL, Ward BK, Ratajczak T. The Calcium-Sensing Receptor: A Molecular Perspective. *Endocr Rev*. 2011;32(1):3-30.

22. Dimke H. New insights into renal calcium-sensing receptor activation. *Curr Opin Nephrol Hypertens*. 2024;33(4):433-440.

23. Zhang J, Li Q, Liao P, et al. Calcium sensing receptor: A promising therapeutic target in pulmonary hypertension. *Life Sci*. Published online 2024:122472.

24. Hannan FM, Kallay E, Chang W, et al. The calcium-sensing receptor in physiology and in calcitropic and noncalcitropic diseases. *Nat Rev Endocrinol*. 2019;15(1):33-51.

25. Chakravarti B, Chattopadhyay N, Brown EM. Signaling Through the Extracellular Calcium-Sensing Receptor (CaSR). In: Islam MdS, ed. *Calcium Signaling*. Advances in Experimental Medicine and Biology. Springer Netherlands; 2012:103-142.

26. Tfelt-Hansen J, Brown EM. The calcium-sensing receptor in normal physiology and pathophysiology: a review. *Crit Rev Clin Lab Sci*. 2005;42(1):35-70.

27. Bircan A, Kuru N, Dereli O, et al. Evolutionary history of calcium-sensing receptors unveils hyper/hypocalcemia-causing mutations. *PLOS Comput Biol*. 2024;20(11):e1012591.

28. Daryadel A, Küng CJ, Haykir B, et al. The calcium-sensing receptor has only a parathyroid hormone-dependent role in the acute response of renal phosphate transporters to phosphate intake. *Am J Physiol-Ren Physiol*. 2024;326(5):F792-F801.

29. Hannan FM, Kallay E, Chang W, et al. Calcium-sensing receptor in physiology and in calcitropic and non-calcitropic diseases. *Nat Rev Endocrinol*. 2018;15(1):33-51.

30. Alfadda TI, Saleh AM, Houillier P, et al. Calcium-sensing receptor 20 years later. *Am J Physiol-Cell Physiol*. 2014;307(3):C221-C231.

31. Brown EM. Role of the calcium-sensing receptor in extracellular calcium homeostasis. *Best Pract Res Clin Endocrinol Metab*. 2013;27(3):333-343.

32. Garrett JE, Capuano IV, Hammerland LG, et al. Molecular cloning and functional expression of human parathyroid calcium receptor cDNAs (∗). *J Biol Chem*. 1995;270(21):12919-12925.

33. Zhang C, Miller CL, Brown EM, et al. The calcium sensing receptor: from calcium sensing to signaling. *Sci China Life Sci*. 2015;58:14-27.

34. Hu J, Spiegel AM. Naturally occurring mutations of the extracellular Ca2+-sensing receptor: implications for its structure and function. *Trends Endocrinol Metab*. 2003;14(6):282-288.

35. Ray K, Adipietro KA, Chen C, et al. Elucidation of the role of peptide linker in calcium-sensing receptor activation process. *J Biol Chem*. 2007;282(8):5310-5317.

36. Bai M, Trivedi S, Lane CR, et al. Protein kinase C phosphorylation of threonine at position 888 in Ca2+ o-sensing receptor (CaR) inhibits coupling to Ca2+ store release. *J Biol Chem*. 1998;273(33):21267-21275.

37. Leach K, Gregory KJ, Kufareva I, et al. Towards a structural understanding of allosteric drugs at the human calcium-sensing receptor. *Cell Res*. 2016;26(5):574-592.

38. Riccardi D, Brown EM. Physiology and pathophysiology of the calcium-sensing receptor in the kidney. *Am J Physiol-Ren Physiol*. 2010;298(3):F485-F499.

39. Breitwieser GE. The calcium sensing receptor life cycle: trafficking, cell surface expression, and degradation. *Best Pract Res Clin Endocrinol Metab*. 2013;27(3):303-313.

40. Bai M, Trivedi S, Brown EM. Dimerization of the extracellular calcium-sensing receptor (CaR) on the cell surface of CaR-transfected HEK293 cells. *J Biol Chem*. 1998;273(36):23605-23610.

41. Gama L, Wilt SG, Breitwieser GE. Heterodimerization of calcium sensing receptors with metabotropic glutamate receptors in neurons. *J Biol Chem*. 2001;276(42):39053-39059.

42. Chen X, Wang L, Cui Q, et al. Structural insights into the activation of human calcium-sensing receptor. *Elife*. 2021;10:e68578.

43. Oldham WM, Hamm HE. Heterotrimeric G protein activation by G-protein-coupled receptors. *Nat Rev Mol Cell Biol*. 2008;9(1):60-71.

44. Conigrave AD, Ward DT. Calcium-sensing receptor (CaSR): pharmacological properties and signaling pathways. *Best Pract Res Clin Endocrinol Metab*. 2013;27(3):315-331.

45. Tuffour A, Kosiba AA, Zhang Y, et al. Role of the calcium-sensing receptor (CaSR) in cancer metastasis to bone: Identifying a potential therapeutic target. *Biochim Biophys Acta BBA - Rev Cancer*. 2021;1875(2):188528.

46. Sundararaman SS, van der Vorst EPC. Calcium-Sensing Receptor (CaSR), Its Impact on Inflammation and the Consequences on Cardiovascular Health. *Int J Mol Sci*. 2021;22(5):2478.

47. Duan K, Mete Ö. Parathyroid carcinoma: diagnosis and clinical implications.

Turk J Pathol. 2015;31.

48. Whitfield JF. Calcium, calcium-sensing receptor and colon cancer. *Cancer Lett*. 2009;275(1):9-16.

49. Casalà C, Gil-Guiñón E, Ordóñez JL, et al. The calcium-sensing receptor is silenced by genetic and epigenetic mechanisms in unfavorable neuroblastomas and its reactivation induces ERK1/2-dependent apoptosis. *Carcinogenesis*. 2013;34(2):268-276.

50. Büsselberg D, Satheesh NJ. Intracellular Calcium in Development and Treatment of Neuroblastoma. In: Vol 2016. HBKU Press Qatar; 2016:HBPP2873.

51. Gregory KJ, Kufareva I, Keller AN, et al. Dual action calcium-sensing receptor modulator unmasks novel mode-switching mechanism. *ACS Pharmacol Transl Sci*. 2018;1(2):96-109.

52. Zhang Y, Fu LJ, Li JX, et al. Gadolinium promoted proliferation and enhanced survival in human cervical carcinoma cells. *Biometals*. 2009;22:511-519.

53. Hwang C, Kang YK, Kim JY, et al. TFE3/PI3K/Akt/mTOR Axis in Renal Cell Carcinoma Affects Tumor Microenvironment. *Am J Pathol*. 2024;194(7):1306-1316.

54. Stelzle D, Tanaka LF, Lee KK, et al. Estimates of the global burden of cervical cancer associated with HIV. *Lancet Glob Health*. 2021;9(2):e161-e169.

55. Perkins RB, Wentzensen N, Guido RS, Schiffman M. Cervical cancer screening: a review. *Jama*. 2023;330(6):547-558.

56. Khairkhah N, Bolhassani A, Najafipour R. Current and future direction in treatment of HPV-related cervical disease. *J Mol Med*. 2022;100(6):829-845.

57. Gennigens C, Jerusalem G, Lapaille L, et al. Recurrent or primary metastatic cervical cancer: current and future treatments. *ESMO Open*. 2022;7(5):100579.

58. Tian L, Andrews C, Yan Q, et al. Molecular regulation of calcium-sensing receptor (CaSR)-mediated signaling. *Chronic Dis Transl Med*. Published online 2024.

59. Peng C, Wang Y, Guo Y, et al. A literature review on signaling pathways of cervical cancer cell death-apoptosis induced by Traditional Chinese Medicine. *J Ethnopharmacol*. Published online 2024:118491.

60. Khan S, Mosvi SN, Vohra S, et al. Implication of calcium supplementations in

health and diseases with special focus on colorectal cancer. *Crit Rev Clin Lab Sci*. Published online 2024:1-14.

61. Tennakoon S, Aggarwal A, Kállay E. The calcium-sensing receptor and the hallmarks of cancer. *Biochim Biophys Acta*. 2016;1863(6 Pt B):1398-1407. doi:10.1016/j.bbamcr.2015.11.017

62. Tu CL, Celli A, Mauro T, et al. Calcium-Sensing Receptor Regulates Epidermal Intracellular Ca2+ Signaling and Re-Epithelialization after Wounding. *J Invest Dermatol*. 2019;139(4):919-929.

63. Alqudah MAY, Azaizeh M, Zayed A, et al. Calcium-Sensing Receptor Antagonist NPS-2143 Inhibits Breast Cancer cell Proliferation, Migration and Invasion via Downregulation of p-ERK1/2, Bcl-2 and Integrin β1 and Induces Caspase 3/7 Activation. *Adv Pharm Bull*. 2022;12(2):383-388. doi:10.34172/apb.2022.037

64. Nie J, Li Q, Yin H, et al. NPS-2143 inhibit glioma progression by suppressing autophagy through mediating AKT–mTOR pathway. *J Cell Mol Med*. 2024;28(7):e18221.

65. Widler L. Calcilytics: antagonists of the calcium-sensing receptor for the treatment of osteoporosis. *Future Med Chem*. 2011;3(5):535-547.

66. Dal Pra I, Armato U, Chioffi F, et al. The Aβ peptides-activated calcium-sensing receptor stimulates the production and secretion of vascular endothelial growth factor-A by normoxic adult human cortical astrocytes. *Neuromolecular Med*. 2014;16:645-657.

67. Palai TK, Mishra SR. Caspases: an apoptosis mediator. *J Adv Vet Anim Res*. 2015;2(1):18-22.

68. Kashyap D, Garg VK, Goel N. Intrinsic and extrinsic pathways of apoptosis: Role in cancer development and prognosis. *Adv Protein Chem Struct Biol*. 2021;125:73-120.

69. Maiellaro I, Barbaro R, Caroppo R, et al. Calcium-sensing receptor signaling: It's all about multiplicity. *Curr Opin Physiol*. 2020;17:243-254.

70. Kosiba AA, Wang Y, Chen D, et al. The roles of calcium-sensing receptor (CaSR) in heavy metals-induced nephrotoxicity. *Life Sci*. 2020;242:117183.

71. Gorvin CM. Recent advances in calcium-sensing receptor structures and

signaling pathways. *Prog Mol Biol Transl Sci*. 2023;195:121-135.

72. Chavez-Abiega S, Mos I, Centeno PP, et al. Sensing extracellular calcium–An insight into the structure and function of the calcium-sensing receptor (CaSR). *Calcium Signal*. Published online 2020:1031-1063.

73. Lang F, Leibrock C, Pelzl L, et al. Therapeutic interference with vascular calcification—lessons from klotho-hypomorphic mice and beyond. *Front Endocrinol*. 2018;9:207.

74. Tomaić V. Functional roles of E6 and E7 oncoproteins in HPV-induced malignancies at diverse anatomical sites. *Cancers*. 2016;8(10):95.

75. Malla R, Kamal MA. E6 and E7 oncoproteins: Potential targets of cervical cancer. *Curr Med Chem*. 2021;28(39):8163-8181.

76. Matthews HK, Bertoli C, de Bruin RA. Cell cycle control in cancer. *Nat Rev Mol Cell Biol*. 2022;23(1):74-88.

77. Wang Z. Regulation of cell cycle progression by growth factor-induced cell signaling. *Cells*. 2021;10(12):3327.

78. Vats A, Trejo-Cerro O, Thomas M, et al. Human papillomavirus E6 and E7: What remains? *Tumour Virus Res*. 2021;11:200213.

79. Orduña-Castillo LB, Del-Río-Robles JE, García-Jiménez I, et al. Calcium sensing receptor stimulates breast cancer cell migration via the Gβγ-AKT-mTORC2 signaling pathway. *J Cell Commun Signal*. 2022;16(2):239-252.

80. Ebrahimi M, Nourbakhsh E, Hazara AZ, et al. PI3K/Akt/mTOR signaling pathway in cancer stem cells. *Pathol-Res Pract*. 2022;237:154010.

81. Yu L, Wei J, Liu P. Attacking the PI3K/Akt/mTOR signaling pathway for targeted therapeutic treatment in human cancer. In: Vol 85. Elsevier; 2022:69-94.

82. Kciuk M, Gielecińska A, Mujwar S, Mojzych M, Kontek R. Cyclin-dependent kinases in DNA damage response. *Biochim Biophys Acta BBA-Rev Cancer*. 2022;1877(3):188716.

83. Abdelrahman KS, Hassan HA, Abdel-Aziz SA, et al. JNK signaling as a target for anticancer therapy. *Pharmacol Rep*. 2021;73:405-434.

84. Koren E, Fuchs Y. Modes of regulated cell death in cancer. *Cancer Discov*.

2021;11(2):245-265.

85. Bossler F, Hoppe-Seyler K, Hoppe-Seyler F. PI3K/AKT/mTOR Signaling Regulates the Virus/Host Cell Crosstalk in HPV-Positive Cervical Cancer Cells. *Int J Mol Sci*. 2019;20(9):2188.

86. Ma C, Gu Y, Liu C, et al. Anti-cervical cancer effects of Compound Yangshe granule through the PI3K/AKT pathway based on network pharmacology. *J Ethnopharmacol*. 2023;301:115820.

87. Patergnani S, Danese A, Bouhamida E, et al. Various aspects of calcium signaling in the regulation of apoptosis, autophagy, cell proliferation, and cancer. *Int J Mol Sci*. 2020;21(21):8323.

88. Chiliquinga AJ, Acosta B, Ogonaga-Borja I, et al. Ion channels as potential tools for the diagnosis, prognosis, and treatment of HPV-Associated cancers. *Cells*. 2023;12(10):1376.

89. Liang R, Liu H, Wang Y, et al. Camkii in Cancer: Molecular Functions and Therapeutic Potential. *Available SSRN 4922125*.

90. Alatise KL, Gardner S, Alexander-Bryant A. Mechanisms of drug resistance in ovarian cancer and associated gene targets. *Cancers*. 2022;14(24):6246.

Acknowledgments

I would like to express my heartfelt gratitude to my supervisor, Professor Anna Chiarini, for her invaluable guidance and mentorship throughout this journey. Her expertise, patience, and unwavering support have been crucial to the successful completion of this dissertation. I am deeply appreciative of her insightful feedback and her dedication to my academic growth.

I also extend my sincere thanks to Professor Ilaria Pierpaola Dal Prà and Professor Ubaldo Armato from the University of Verona, as well as Professor Wu Jun, Director of the Department of Burns and Plastic Surgery at the Second People's Hospital of Shenzhen, and Professor Yin Meifang. Their thoughtful comments and suggestions have significantly enhanced the quality and direction of my research.

My gratitude also goes to Professor Wei Zairong, Professor Deng Chengliang, and Professor Wang Dali, along with the entire Burn and Plastic Surgery team at Zunyi Medical University. Their constant support and encouragement have been a pillar of strength for me, helping me overcome various challenges. Their guidance, both technical and personal, has been instrumental in shaping my academic and professional development.

Lastly, I owe my deepest thanks to my wife, Zhao Qian. Her love, patience, and understanding have been essential throughout this demanding journey. During times of uncertainty and exhaustion, she was always there, offering unwavering support. Her belief in me has been a source of constant motivation, and I am truly grateful for all she has done.